Eur. Phys. J. A (2023) 59:223
https://doi.org/10.1140/epja/s10050-023-01131-3

THE EUROPEAN PHYSICAL JOURNAL A

Regular Article - Theoretical Physics

The electromagnetic fine-structure constant in primordial nucleosynthesis revisited

Ulf-G. Meißner[1,2,3,4,5,a], **Bernard Ch. Metsch**[1,3,b], **Helen Meyer**[1,2,c]

[1] Helmholtz-Institut für Strahlen- und Kernphysik, Rheinische Friedrich-Wilhelms Universität Bonn, D-53115 Bonn, Germany
[2] Bethe Center for Theoretical Physics, Rheinische Friedrich-Wilhelms Universität Bonn, 53115 Bonn, Germany
[3] Institute for Advanced Simulation (IAS-4), Forschungszentrum Jülich, 52425 Jülich, Germany
[4] Institut für Kernphysik (IKP-3) and Jülich Center for Hadron Physics, Forschungszentrum Jülich, 52425 Jülich, Germany
[5] Tbilisi State University, 0186 Tbilisi, Georgia

Received: 12 July 2023 / Accepted: 20 September 2023 / Published online: 4 October 2023

Communicated by Jérôme Margueron

Abstract We study the dependence of the primordial nuclear abundances as a function of the electromagnetic fine-structure constant α, keeping all other fundamental constants fixed. We update the leading nuclear reaction rates, in particular the electromagnetic contribution to the neutron-proton mass difference pertinent to β-decays, and go beyond certain approximations made in the literature. In particular, we include the temperature-dependence of the leading nuclear reactions rates and assess the systematic uncertainties by using four different publicly available codes for Big Bang nucleosynthesis. Disregarding the unsolved so-called lithium-problem, we find that the current values for the observationally based ^{2}H and ^{4}He abundances restrict the fractional change in the fine-structure constant to less than 2%, which is a tighter bound than found in earlier works on the subject.

1 Introduction

Since the early work of Dirac [1], variations of the fundamental constants of physics have been considered in a variety of scenarios, see [2] for a recent status report on possible spatial and temporal variations of the electromagnetic fine-structure constant α, the gravitational constant G and the ratio of the proton and electron masses, μ_p. See also the recent review [3].

As is well known, primordial or Big Bang nucleosynthesis (BBN) is a fine laboratory to test our understanding of the fundamental physics describing the generation of the light elements. In particular, it sets bounds on the possible variation of the parameters of the Standard Model of particle physics as well as the Standard Model of cosmology (ΛCDM). For recent reviews, see *e.g.* Refs. [4–6]. Here, we are interested in bounds on the electromagnetic fine-structure constant α derived from the element abundances in primordial nucleosynthesis. For earlier work on this topic, see *e.g.* [7–10] and references therein. This work is part of a larger program that tries to map out the habitable universes in the sense that the pertinent nuclei needed to generate life as we know it are produced in the Big Bang and in stars in a sufficient amount, see *e.g.* [11,12] for reviews.

Here, we focus largely on the nuclear and particle physics underlying the element generation in primordial nucleosynthesis. In particular, we reassess the dependence of the nuclear reactions rates on the fine-structure constant, overcoming on one side certain approximations made in the literature and on the other side providing new and improved parameterizations for the most important reactions in the reaction network, using modern determinations of the ingredients whenever possible, such as the Effective Field Theory (EFT) description of the leading nuclear reaction $n + p \to d + \gamma$[1] and the calculation of the nuclear Coulomb energies based on Nuclear Lattice Effective Field Theory. For β-decays, we also use up-to-date information on the neutron-proton mass difference based on dispersion relations (Cottingham sum rule). Most importantly, as already done in Ref. [19], we utilize four different publicly available codes for BBN [20–26]

[a] e-mail: meissner@hiskp.uni-bonn.de
[b] e-mail: metsch@hiskp.uni-bonn.de (corresponding author)
[c] e-mail: hmeyer@hiskp.uni-bonn.de

[1] There are some *ab initio* calculations of other reactions in the BBN network such as [13–18], mainly concerned with radiative capture reactions. The calculations in the framework of so-called "halo-EFT" potentially offer the possibility to study the α dependence of the cross sections analytically, but the implementation is numerically rather involved and we thus refrained from doing so in the present context.

to address the systematic uncertainties related to the modelling of the BBN network. In particular these codes differ in the number of nuclei and reactions taken into account as well as in the specific parameterization of the nuclear rates entering the coupled rate equations for the BBN network. Moreover, in determining the sensitivity of primordial abundances on nuclear parameters, we account for the temperature dependence of the variation of some rates on the value of the fine-structure constant α. To our knowledge, such a comparative study where this temperature dependence was explicitly considered for a variation of α has not been published before. We further note that we keep all other constants, like *e.g.* the light quark masses m_u, m_d fixed at their physical values.

The paper is organized as follows: In Sect. 2 we collect the basic formulas needed for discussing the fine-structure constant dependence in BBN. In this section we discuss the various dependences of the reaction rates on the value of the electromagnetic fine-structure constant α. The actual calculation of the reaction rates is treated in Sect. 3. The BBN response matrix is introduced in Sect. 4. The numerical results of this study are presented in Sect. 5 and discussed in Sect. 6. We also present a detailed comparison to results obtained in earlier works. In Appendix A we give the novel parameterizations of 18 leading nuclear reactions in the BBN network.

2 Basic formalism

As discussed in Ref. [19], the basic quantities to be determined in BBN are the nuclear abundances Y_{n_i}, where n_i denotes some nuclide. The evolution of the nuclear abundance Y_{n_1} is then generically given by

$$\dot{Y}_{n_1} = \sum_{\substack{n_2,\ldots,n_p \\ m_1,\ldots,m_q}} N_{n_1} \left(\Gamma_{m_1,\ldots,m_q \to n_1,\ldots n_p} \frac{Y_{m_1}^{N_{m_1}} \cdots Y_{m_q}^{N_{m_q}}}{N_{m_1}! \cdots N_{m_q}!} - \Gamma_{n_1,\ldots,n_p \to m_1,\ldots m_q} \frac{Y_{n_1}^{N_{n_1}} \cdots Y_{n_p}^{N_{n_p}}}{N_{n_1}! \cdots N_{n_p}!} \right) , \tag{1}$$

where the dot denotes the time derivative in a comoving frame, and N_{n_i} is the stochiometric coefficient of species n_i in the reaction. Further, for a two-particle reaction $a + b \to c + d$, $\Gamma_{ab\to cd} = n_B \gamma_{ab\to cd}$ is the reaction rate with n_B the baryon volume density. This can readily be generalised to reactions involving more (or less) particles, see [26]. These equations are coupled via the corresponding energy densities to the standard Friedmann equation describing the cosmological expansion in the early universe, for details and basic assumptions, see also [22,25,26]. In what follows, we discuss the various types of reactions in the BBN network and their dependence on the electromagnetic fine-structure constant.

2.1 Reaction rates

The average reaction rate $\gamma_{ab\to cd} = N_A \langle \sigma_{ab\to cd}\, v \rangle$ for a two-particle reaction $a + b \to c + d$ is obtained by folding the cross section $\sigma_{ab\to cd}(E)$ with the Maxwell-Boltzmann velocity distribution in thermal equilibrium

$$\gamma_{ab\to cd}(T) = N_A \sqrt{\frac{8}{\pi \mu_{ab} (kT)^3}} \int_0^\infty \mathrm{d}E\, E\, \sigma_{ab\to cd}(E) \times \mathrm{e}^{-\frac{E}{kT}} , \tag{2}$$

conventionally multiplied by Avogadro's number N_A, where μ_{ij} is the reduced mass of the nuclide pair ij, $\mu_{ij} = m_i m_j/(m_i + m_j)$, E is the kinetic energy in the center-of-mass system (CMS), T is the temperature and k the Boltzmann constant. Defining $y = E/(kT)$ this can be written in the form

$$\gamma_{ab\to cd}(T) = N_A \sqrt{\frac{8\,kT}{\pi\, \mu_{ab}}} \int_0^\infty \mathrm{d}y\, \sigma_{ab\to cd}(kTy)\, y\, \mathrm{e}^{-y} . \tag{3}$$

This is suited for numerical computation *e.g.* with a Gauß-Laguerre integrator. In fact, in order to deal with cases with singular cross sections for $E \to 0$ it is even better to split the integral and write

$$\int_0^\infty \mathrm{d}y\, \sigma(kTy)\, y\, \mathrm{e}^{-y} = 2 \int_0^{\sqrt{\overline{y}}} \mathrm{d}x\, \sigma(kTx^2)\, x^3\, \mathrm{e}^{-x^2} + \int_{\overline{y}}^\infty \mathrm{d}y\, \sigma(kTy)\, y\, \mathrm{e}^{-y} \tag{4}$$

and evaluate the first integral with a Gauß-Legendre and the second with a Gauß-Laguerre integrator for some suitable value of $\overline{y}$. Note that in the first term the substitution $x = \sqrt{y}$ was performed.

With the detailed balance relation

$$\sigma_{cd\to ab}(E') = \frac{g_a\, g_b}{g_c\, g_d} \frac{p^2}{p'^2} \sigma_{ab\to cd}(E) , \tag{5}$$

where

$$E = \frac{p^2}{2\,\mu_{ab}} , \quad E' = \frac{p'^2}{2\,\mu_{cd}} , \tag{6}$$

are the CMS kinetic energies in the entrance and exit channels, respectively, and g_i is the spin multiplicity of particle i, energy conservation implies

$$m_a + m_b + E = m_c + m_d + E' \quad \text{or} \quad E' = E + Q , \text{ with } Q = m_a + m_b - m_c - m_d , \tag{7}$$

in terms of the Q-value for the forward reaction. In thermal equilibrium the inverse reaction rate is then related to the forward rate as

$$\gamma_{cd\to ab}(T) = \left(\frac{\mu_{ab}}{\mu_{cd}}\right)^{\frac{3}{2}} \frac{g_a\, g_b}{g_c\, g_d}\, \mathrm{e}^{-\frac{Q}{kT}}\, \gamma_{ab\to cd}(T)\,. \tag{8}$$

This brings us to the central question of this paper, namely how the value of the electromagnetic fine-structure constant

$$\alpha = \frac{e^2}{\hbar c} \tag{9}$$

influences the reaction rates? This clearly depends on the reaction type. With the exception of the leading $n + p \to d + \gamma$ nuclear reaction, to be discussed in some detail below, no *ab initio* expressions for most of the reaction cross sections is available and accordingly one has to rely on model assumptions concerning the fine-structure constant dependence of the cross sections and thus of the reaction rates (see also the discussion in Sect. 6 on this issue). These shall be discussed in the following subsections separately for *strong reactions* of the type

$$a + b \to c + d\,, \tag{10}$$

radiative capture reactions of the type

$$a + b \to c + \gamma\,, \tag{11}$$

and β*-decays*,

$$a \to c + e^{\mp} + \overset{(-)}{\nu}\,. \tag{12}$$

Note that in the considerations that follow we concentrate on modeling the impact of a variation of α on the penetrability, related to the Coulomb interaction between charged particles, as well as on the changes in reaction Q-values due to changes in binding energies of the nuclides involved in the reaction. Some of the reactions show appreciable resonance contributions, see *e.g.* those listed in Table 11 of the appendix, and the corresponding resonance parameters (*viz.* excitation energy (position) and width) in principle also depend on the value of α. The study of these effects would, as already mentioned above, require a detailed theoretical description of the nuclear structure and reaction dynamics of the nuclides involved, see *e.g.* Refs. [48–51] for results in the framework of NLEFT. Such a treatment we considered to be beyond the scope of the present study and accordingly we shall assume that resonance parameters are α-independent.

We shall start with a brief discussion of the Coulomb penetration factor for charged particles, relevant for what follows.

2.1.1 *Coulomb-penetration factor*

The Coulomb-penetration factor for an ℓ-wave is given by, see *e.g.* [27,28],

$$v_\ell(\eta, \rho) = \frac{1}{F_\ell^2(\eta, \rho) + G_\ell^2(\eta, \rho)}\,, \tag{13}$$

where $F_\ell\,, G_\ell$ are the regular and irregular Coulomb functions, respectively, that are the linearly independent solutions of the radial Schrödinger equation

$$u_\ell''(\rho) + \left(1 - \frac{2\,\eta}{\rho} - \frac{\ell(\ell+1)}{\rho^2}\right) u_\ell(\rho) = 0\,, \tag{14}$$

where we defined

$$\begin{aligned} k &= \sqrt{\frac{2\,\mu_{ab}c^2\,E}{\hbar^2 c^2}}\,,\\ \rho &= k\,r\,,\\ \eta &= \frac{Z_a\,Z_b\,\mu_{ab}c^2\,\alpha}{\hbar c\,k}\,, \end{aligned} \tag{15}$$

for the Coulomb-scattering of charges $Z_a e\,,\ Z_b e$ with masses $m_a\,, m_b$ and the reduced mass

$$\mu_{ab} = \frac{m_a\,m_b}{m_a + m_b} \tag{16}$$

at the energy E of the relative motion, subject to the Coulomb-potential

$$V(r) = \frac{Z_a\,Z_b\,e^2}{r} = \frac{Z_a\,Z_b\,\alpha\,\hbar c}{r}\,. \tag{17}$$

Approximate parameterizations of $v_\ell(\eta, \rho)$ have been extensively discussed in the literature, see *e.g.* [29] in particular for the dependence on the nuclear distance r where this is to be evaluated for a specific reaction. As argued in [27,28], this distance is not well defined and the cross section should not depend on such an unobservable parameter. Accordingly, if one takes, as in [27,28], $\lim \rho \to 0$ the penetration factor for an ℓ-wave then reads

$$\begin{aligned} v_\ell(\eta) &\approx \varepsilon_\ell^2\,,\\ \varepsilon_\ell^2 &= \left(1 + \frac{\eta^2}{\ell^2}\right)\varepsilon_{\ell-1}^2\,,\\ \varepsilon_0^2 &= \frac{2\pi\,\eta}{\mathrm{e}^{2\pi\,\eta} - 1}\,. \end{aligned} \tag{18}$$

Therefore, we shall use as Coulomb penetration factor the expression for s-waves:

$$P(x) = \frac{x}{\mathrm{e}^x - 1}\,, \quad \lim_{x\to 0} P(x) = 1\,. \tag{19}$$

Note that the corrections due to a variation of α in ε_ℓ^2 for $\ell > 0$ according to Eq. (18) are of higher order in α and thus

small anyway. Here we defined

$$x = 2\pi \, \frac{Z_a \, Z_b \, \mu_{ab} c^2 \, \alpha}{\hbar c \, k} = \sqrt{\frac{E_G(\alpha)}{E}} \tag{20}$$

in terms of the so-called Gamow energy for a two-particle reaction channel ij

$$E_G(\alpha) = 2\,\pi^2 \, Z_i^2 \, Z_j^2 \, \mu_{ij} c^2 \, \alpha^2 \tag{21}$$

and the CMS energy E or $E + Q$ for the entrance and exit channel, respectively.

2.2 Strong reactions $a + b \to c + d$

For a strong reaction of this type the Q-value is given by

$$Q = m_a + m_b - m_c - m_d \, , \tag{22}$$

where the nuclear mass of each nuclide i with mass number A_i and charge number Z_i reads

$$m_i = Z_i \, m_p + (A_i - Z_i) \, m_n - B_i \, , \tag{23}$$

with B_i the nuclear binding energy. Thus, because of baryon number and charge conservation ($A_a + A_b = A_c + A_d$, $Z_a + Z_b = Z_c + Z_d$):

$$Q = B_c + B_d - B_a - B_b \, . \tag{24}$$

Now the binding energy can be written as

$$B_i = B_i^N - V_i^C(\alpha) \, , \tag{25}$$

where B_i^N denotes the strong contribution to the binding energy and

$$V_i^C(\alpha) \propto \alpha \, Z_i \, (Z_i - 1) \tag{26}$$

is the expectation value of the Coulomb contribution proportional to the value of the electromagnetic fine-structure constant. Considering its variation in the form $\alpha = \alpha_0 \, (1 + \delta_\alpha)$, where

$$\alpha_0 = 7.2973525693(11) \, 10^{-3} = 1/137.035999084(2) \tag{27}$$

is the current experimental value from Ref. [30], the Q-value varies as

$$Q(\alpha) = Q(\alpha_0) + (V_a^C + V_b^C - V_c^C - V_d^C) \, \delta_\alpha \, . \tag{28}$$

One therefore needs an estimate of the Coulomb contribution to the nuclear masses, this we shall discuss in Sect. 2.7.

We shall assume that the cross section for a strong reaction $a + b \to c + d$ depends on α as

$$\sigma_{ab\to cd}\left(E;\, Q(\alpha),\, E_G^i(\alpha),\, E_G^i(\alpha)\right) = \sqrt{E + Q(\alpha)} \, P_i(x_i(E,\alpha)) \, P_f(x_f(E,\alpha)) \, f(E) \, , \tag{29}$$

where f is some function independent of α and $P_i(x_i)$, $P_f(x_f)$ are the penetration factors given by Eq. (19) reflecting the Coulomb repulsion in the entrance and in the exit channel, respectively. The first factor in Eq. (29) accounts for the exit channel momentum dependence of the cross section of the strong reaction $a + b \to c + d$. Here,

$$x_i(E,\alpha) = \sqrt{\frac{E_G^i(\alpha)}{E}} \, , \tag{30}$$

$$x_f(E,\alpha) = \sqrt{\frac{E_G^f(\alpha)}{E + Q(\alpha)}} \, , \tag{31}$$

are the arguments of the penetration factors, with

$$E_G^i(\alpha) = 2\,\pi^2 \, Z_a^2 \, Z_b^2 \, \mu_{ab} c^2 \, \alpha^2 \, , \tag{32}$$

$$E_G^f(\alpha) = 2\,\pi^2 \, Z_c^2 \, Z_d^2 \, \mu_{cd} c^2 \, \alpha^2 \, , \tag{33}$$

the Gamow-energies in the entrance and the exit channel, respectively, and $\mu_{ij} = m_i \, m_j/(m_i + m_j)$ the corresponding reduced masses. Although in order to calculate the linear response of the abundances one could proceed by calculating first order partial derivatives

$$\frac{\partial \sigma}{\partial \alpha} = \frac{\partial \sigma}{\partial Q} \, \frac{\partial Q}{\partial \alpha} + \sum_{k=i,\,f} \frac{\partial \sigma}{\partial P_k} \, \frac{\partial P_k}{\partial x_k} \, \frac{\partial x_k}{\partial \alpha} \, , \tag{34}$$

etc., we prefer not to presume linearity and rather calculate a variation of the cross section with a variation $\alpha = \alpha_0 \, (1 + \delta_\alpha)$ through the expression

$$\begin{aligned} &\sigma_{ab\to cd}\left(E;\, Q(\alpha),\, E_G^f(\alpha),\, E_G^i(\alpha)\right) \\ &\quad = \sigma_{ab\to cd}\left(E;\, Q(\alpha_0),\, E_G^i(\alpha_0),\, E_G^f(\alpha_0)\right) \\ &\qquad \times \frac{P(x_i(E,\alpha))}{P(x_i(E,\alpha_0))} \sqrt{\frac{E + Q(\alpha)}{E + Q(\alpha_0)}} \, \frac{P(x_f(E,\alpha))}{P(x_f(E,\alpha_0))} \, , \end{aligned} \tag{35}$$

where specifically the first factor reads

$$\begin{aligned} \frac{P(x_i(E,\alpha))}{P(x_i(E,\alpha_0))} &= \frac{\sqrt{\frac{E_G^i(\alpha)}{E}}}{\mathrm{e}^{\sqrt{\frac{E_G^i(\alpha)}{E}}} - 1} \, \frac{\mathrm{e}^{\sqrt{\frac{E_G^i(\alpha_o)}{E}}} - 1}{\sqrt{\frac{E_G^i(\alpha_0)}{E}}} \\ &= \begin{cases} 1, & \text{for } n\text{-induced reactions} \\ (1 + \delta_\alpha) \, \frac{\mathrm{e}^{\sqrt{\frac{E_G^i(\alpha_o)}{E}}} - 1}{\mathrm{e}^{\sqrt{\frac{E_G^i(\alpha)}{E}}} - 1} \, , & \text{else,} \end{cases} \end{aligned} \tag{36}$$

and the remaining factors are given by

$$\sqrt{\frac{E + Q(\alpha)}{E + Q(\alpha_0)}} \, \frac{P(x_f(E,\alpha))}{P(x_f(E,\alpha_0))}$$

$$= \begin{cases} \sqrt{\frac{E+Q(\alpha)}{E+Q(\alpha_0)}}\,, & \text{if } c = n \text{ and/or } d = n \\ \sqrt{\frac{E_G^f(\alpha)}{E_G^f(\alpha_0)}}\,\frac{e^{\sqrt{\frac{E_G^f(\alpha_0)}{E+Q(\alpha_0)}}}-1}{e^{\sqrt{\frac{E_G^f(\alpha)}{E+Q(\alpha)}}}-1}\,, & \text{else.} \end{cases} \tag{37}$$

We note that these factors are energy-dependent and therefore the change in the rate

$$\gamma(T;\, Q(\alpha), E_G^i(\alpha), E_G^f(\alpha)) = \int_0^\infty \mathrm{d}E\; E\,\sigma(E;\, Q(\alpha), E_G^i(\alpha), E_G^f(\alpha))\; e^{-\frac{E}{kT}}\,, \tag{38}$$

i.e. the factor

$$\frac{\gamma(T;\, Q(\alpha), E_G^i(\alpha), E_G^f(\alpha))}{\gamma(T;\, Q(\alpha_0), E_G^i(\alpha_0), E_G^f(\alpha_0))} \tag{39}$$

depends on the temperature T and as it stands requires a numerical evaluation of Eq. (38).

2.3 Radiative capture reactions $a + b \to c + \gamma$

Similar considerations hold for radiative capture reactions. The cross section of a reaction $a + b \to c + \gamma$ is assumed to depend on α as

$$\sigma_{ab\to c\gamma}(E;\, Q(\alpha), E_G^i(\alpha)) = \alpha\,(E + Q(\alpha))^3\, P_i(x_i(E,\alpha))\, f(E) \tag{40}$$

with f some α-independent function and $P_i(x_i)$ the penetration factor, see Eqs. (19,30,32), for the entrance channel. The first factor accounts for the fact that in the amplitude for a radiative capture reaction the photon coupling is proportional to e, leading to a factor proportional to $\alpha = e^2/(\hbar c)$ in the cross section. The second factor reflects the final momentum dependence assuming dipole dominance of the radiation [2]. We thus calculate a variation of the cross section for radiative capture with a variation $\alpha = \alpha_0\,(1 + \delta_\alpha)$ via

$$\sigma_{ab\to c\gamma}\left(E;\, Q(\alpha), E_G^i(\alpha)\right) = \sigma_{ab\to c\gamma}\left(E;\, Q(\alpha_0), E_G^i(\alpha_0)\right) \times \frac{P(x_i(E,\alpha))}{P(x_i(E,\alpha_0))}\,(1+\delta_\alpha)\left(\frac{E+Q(\alpha)}{E+Q(\alpha_0)}\right)^3 \tag{41}$$

where the first factor is the same as in Eq. (36). Again note that both factors are energy-dependent and therefore a change in the rate, see Eq. (38), is temperature-dependent.

[2] Note, however, that this is not always the case, exceptions with appreciable $E2$ (electric quadrupole) contributions are *e.g.* the reactions: $^2\mathrm{H}+^2\mathrm{H} \to {}^4\mathrm{He}+\gamma$, $^2\mathrm{H}+^4\mathrm{He} \to {}^6\mathrm{Li}+\gamma$ and $^4\mathrm{He}+^{12}\mathrm{O} \to {}^{16}\mathrm{O}+\gamma$. We nevertheless always assume dipole dominance.

2.4 Approximate treatment of α-dependent factors

As mentioned twice, the variation of the cross sections with a variation of α induces energy-dependent factors, that in turn lead to temperature-dependent variations in the corresponding reaction rates, that can be fully accounted for only via a numerical integration of Eq. (38). In fact this is what was done in the present work for the most important 18 nuclear reactions in the BBN network, listed in Sect. 5. For the remaining reactions we relied on the following approximations, that turned out to be effective.

For neutron induced reactions

$$\sigma(E) \propto \frac{R(E)}{\sqrt{E}} \tag{42}$$

where for a non-resonant reaction $R(E)$ is a weakly dependent function of the CMS kinetic energy E, see *e.g.* [31]. If we make the extreme approximation that $R(E) \approx const.$ the maximum of the remaining energy dependent factors in the integrand of Eq. (38) is reached at the energy

$$E = \overline{E}_n = \frac{1}{2}\,kT\,. \tag{43}$$

Likewise, assuming that for the astrophysical S-factor for charged particle induced reactions

$$S(E) = E\,\sigma(E)\,e^{\sqrt{\frac{E_G^i}{E}}} \approx const. \tag{44}$$

holds, one finds that the maximum of the remaining energy-dependent factors in the rate is reached at

$$E = \overline{E}_c = \left(\frac{kT}{2}\right)^{\frac{2}{3}} (E_G^i)^{\frac{1}{3}}\,. \tag{45}$$

Substituting $E \mapsto \overline{E}_n, \overline{E}_c$ in the expressions in Eqs. (35, 41) then leads to temperature-dependent factors, that can be taken in front of the integral in Eq. (38) and thus merely multiply the corresponding rates. The quality of this approximation may be inferred from Fig. 1, where we compare the results of the numerical calculation of the rates according to Eq. (38) (yellow areas for a variation $\delta_\alpha \in [-0.1, 0.1]$) with the approximation discussed in this subsection, represented by blue lines for $\delta_\alpha = -0.1$ and 0.1.

Note that in the present treatment we preferred to account for the Coulomb suppression in an entrance or exit channel with charged particles by the penetration factor of Eq. (19) and do not rely on a simple Gamow-factor $\propto e^{-x} = e^{-\sqrt{E_G(\alpha)/E}}$, with E being the CMS energy of the relevant channel with charged particles. We found that doing so would lead to overestimating the α-dependence in the rates by a factor ≈ 1.5, while the temperature dependence would still roughly follow the same trends as in Fig. 1.

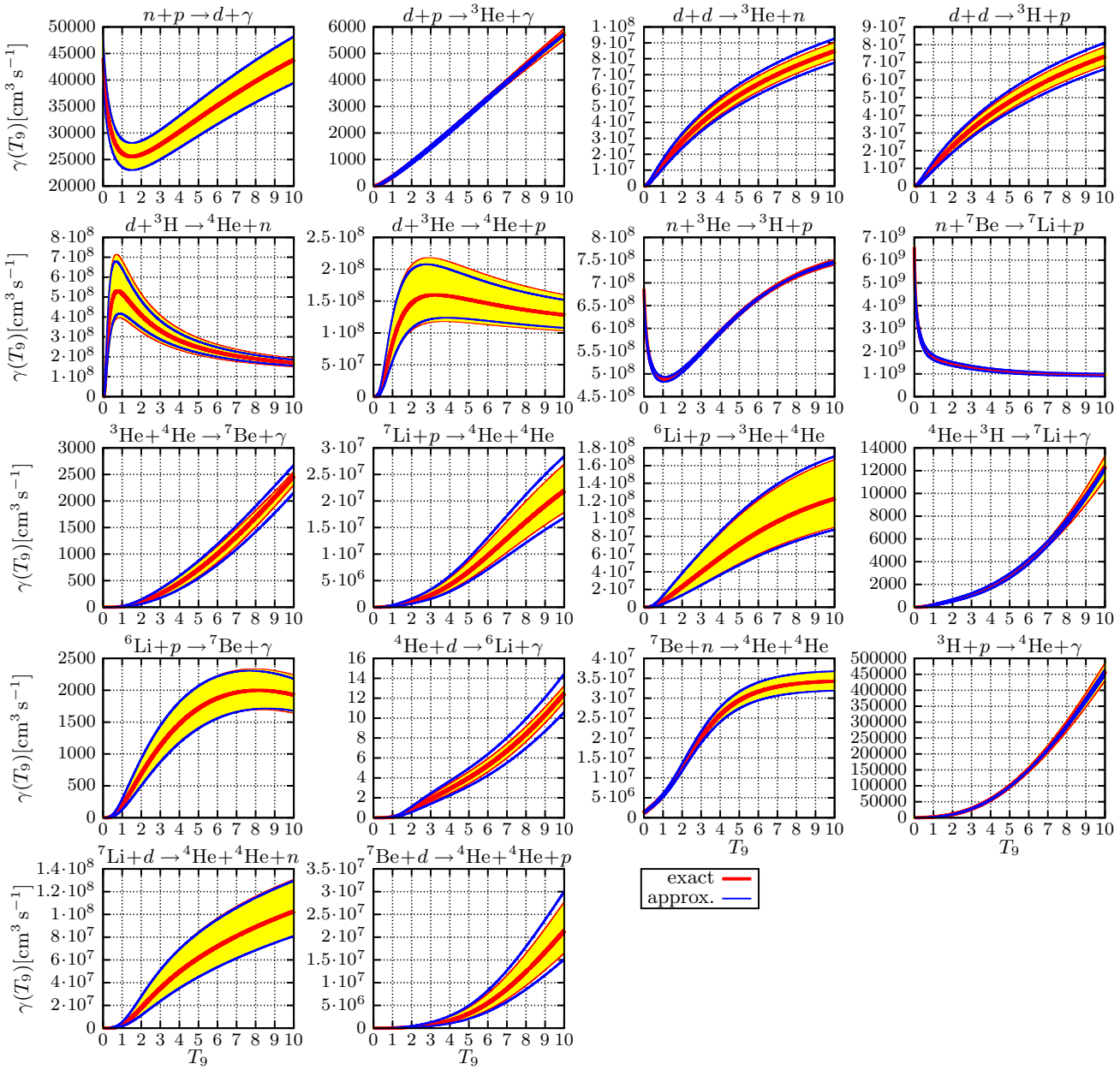

Fig. 1 Temperature-dependence ($T_9 = T/10^9$ K) of the variation of the rates γ of 18 leading nuclear reactions with a variation of the fine structure constant $\alpha = \alpha_0\,(1+\delta_\alpha)$. Shown are the exact results in the interval $\delta_\alpha = [-0.1, 0.1]$ (yellow area, color online) bounded by the curves (in red) at $\delta_\alpha = -0.1$ and 0.1 as well as the approximate expression discussed in Sect. 2.4 for $\delta_\alpha = -0.1$ and 0.1 (blue curves)

2.5 Coulomb-effects in β-decays

Next, we consider the various β-decays in the BBN network. The rate for β-decays $a \to c + e^{\pm} + \overset{(-)}{\nu}$ can be written as, see *e.g.* [32],

$$\lambda = \frac{G^2}{2\pi^3}\,\frac{m_p\,c^2}{\hbar}\,|\mathcal{M}_{ac}|^2\;f(Z,q)\,, \tag{46}$$

where G is Fermi's weak coupling constant, $\mathcal{M}_{ac}$ the nuclear matrix element and

$$f(\pm Z,q) = \int_1^q \mathrm{d}x\;F(\pm Z,x)\,\sqrt{x^2-1}\,x\,(q-x)^2\,, \tag{47}$$

see Eq. (2.158) of Ref. [33], where we defined $q = Q/m_e = (m_a - m_c)/m_e$. Further, $F(\pm Z, E)$ is the so-called Fermi-function

$$F(\pm Z,E) = F_0(\pm Z,E)\,L_0(\pm Z,E)\,,$$

$$
\begin{aligned}
L_0(\pm Z, E) &= \frac{1+\gamma}{2} \mp \frac{5}{3}\,\alpha\, Z\, R\, E \mp \frac{\alpha\, Z\, R}{3\, E} \\
&\quad -\frac{1}{3}\,(E^2-1)\,R^2 + \cdots\,, \\
F_0(\pm Z, E) & \\
&= 4\,(2\sqrt{E^2-1}\,R)^{2\gamma-2}\,\mathrm{e}^{\pm\pi\nu}\,\frac{|\Gamma(\gamma \pm \mathrm{i}\,\nu)|^2}{(\Gamma(2\gamma+1))^2}
\end{aligned}
\tag{48}
$$

with the definitions

$$
\begin{aligned}
\gamma &= \sqrt{1-(Z\,\alpha)^2}\,, \\
\nu &= \frac{Z\,\alpha\, E}{\sqrt{E^2-1}}\,,
\end{aligned}
\tag{49}
$$

where Z is the atomic number of the daughter nucleus c and R its radius, see Eqs. (2.121)-(2.125),(2.131) of Ref. [33]. The upper/lower sign holds for β^-/β^+ decays, respectively. For $Z\,\alpha \ll 1$ we can approximate

$$
\begin{aligned}
&\gamma \approx 1\,, \quad L_0(\pm Z, E) \approx 1\,, \\
&F_0(\pm Z, E) \approx 4 \cdot 1 \cdot \mathrm{e}^{\pm\pi\nu}\,\frac{|\Gamma(1 \pm \mathrm{i}\,\nu)|^2}{4}
\end{aligned}
\tag{50}
$$

or, with $|\Gamma(1 \pm \mathrm{i}\,\nu)|^2 = \pm\pi\,\nu/\sinh(\pm\pi\,\nu)$

$$
F_0(\pm Z, E) \approx \frac{\pm 2\pi\,\nu\,\mathrm{e}^{\pm\pi\nu}}{\mathrm{e}^{\pm\pi\nu} - \mathrm{e}^{\mp\pi\nu}} = \frac{\pm 2\pi\,\nu}{1-\mathrm{e}^{\mp 2\pi\,\nu}}\,,
\tag{51}
$$

such that $\lim_{Z\to 0} F_0(\pm Z, E) = 1$. Accordingly, setting $a = 2\pi\,Z\,\alpha$ then

$$
\begin{aligned}
f(\pm Z, q) &= \int_1^q \mathrm{d}x\; \frac{\pm\frac{a\,x}{\sqrt{x^2-1}}}{1-\mathrm{e}^{\mp\frac{a\,x}{\sqrt{x^2-1}}}}\,\sqrt{x^2-1}\,x\,(q-x)^2 \\
&= \int_1^q \mathrm{d}x\; \frac{\pm a\,x^2}{1-\mathrm{e}^{\mp\frac{a\,x}{\sqrt{x^2-1}}}}\,(q-x)^2\,.
\end{aligned}
\tag{52}
$$

Defining also $p = \sqrt{q^2-1}$ (*i.e.* the maximal momentum in β-decay divided by the electron mass) and with the substitution $y = \sqrt{x^2-1}/p$ we can rewrite the expression for $f(\pm Z, q)$ as

$$
\begin{aligned}
f(\pm Z, p) &= f(\pm a, p) \\
&= \pm a\,p^2 \int_0^1 \mathrm{d}y\; y\,\frac{\sqrt{1+p^2\,y^2}}{1-\mathrm{e}^{\mp\frac{a\sqrt{1+p^2\,y^2}}{p\,y}}} \\
&\quad \times \left(\sqrt{1+p^2} - \sqrt{1+p^2\,y^2}\right)^2\,,
\end{aligned}
\tag{53}
$$

which is slightly better suited for a numerical implementation, *e.g.* with a Gauß-Legendre-integrator. Note that both a and p depend on α.

2.5.1 Electromagnetic contribution to the proton-neutron mass difference

The neutron-proton mass difference plays an important role in BBN, see *e.g.* [41]. According to Refs. [34,35] the proton-neutron mass difference is given by

$$
\begin{aligned}
m_p - m_n &= \Delta m = \Delta m_{\mathrm{QCD}} + \Delta m_{\mathrm{QED}}\,, \\
\Delta m_{\mathrm{QCD}} &= -1.87 \mp 0.16\,\mathrm{MeV}\,, \\
\Delta m_{\mathrm{QED}} &= 0.58 \pm 0.16\,\mathrm{MeV}\,,
\end{aligned}
\tag{54}
$$

where the nominal electromagnetic contribution is somewhat smaller than the value $\Delta m_{\mathrm{QED}} = 0.7 \pm 0.3\,\mathrm{MeV}$ given earlier in Ref. [36]. We also note that the splitting in strong and electromagnetic contributions is convention-dependent, for a pedagogical discussion see [37]. For a comparison of these results with lattice QCD and other phenomenological determinations of the electromagnetic contribution to the neutron-proton mass difference, we refer to [34].

The neutron-proton mass difference is a crucial parameter both in the various $n \leftrightarrow p$ weak interactions in the early phase of BBN and in all β-decays. We shall start with a discussion of the latter.

2.5.2 Implications for β-decays

Writing

$$
m_n - m_p = -(\Delta m_{\mathrm{QCD}} + \Delta m_{\mathrm{QED}})\,,
\tag{55}
$$

the Q-value for the β-decay $a \to c + e^{\mp} + \overset{(-)}{\nu}_e$ depends on a variation of $\alpha = \alpha_0(1+\delta_\alpha)$ as

$$
\begin{aligned}
Q(\alpha) &= Q(\alpha_0(1+\delta_\alpha)) \\
&= \pm(-\Delta m_{\mathrm{QCD}} - \Delta m_{\mathrm{QED}}\,(1+\delta_\alpha)) \\
&\quad -(B_a^N - V_a^C\,(1+\delta_\alpha)) \\
&\quad +(B_c^N - V_c^C\,(1+\delta_\alpha)) \\
&= Q(\alpha_0) + (V_a^C - V_c^C \mp \Delta m_{\mathrm{QED}})\,\delta_\alpha\,,
\end{aligned}
\tag{56}
$$

where, as in Sect. 2.2, B_i^N is the nuclear (strong) contribution to the binding energy of nuclide i and V_i^C the expectation value of the Coulomb-interaction to the binding energy of nuclide i.

One thus finds for the variation of the β-decay rate with a variation of α,

$$
\lambda(\alpha_0\,(1+\delta_\alpha)) = \lambda(\alpha_0)\,\frac{f(\tilde{a}(\delta_\alpha), \tilde{p}(\delta_\alpha))}{f(a,p)}\,,
\tag{57}
$$

where

$$
\begin{aligned}
\tilde{a}(\delta_\alpha) &= a\,(1+\delta_\alpha)\,, \\
\tilde{p}(\delta_\alpha) &= \sqrt{\tilde{q}^2(\delta_\alpha) - 1}\,, \\
\tilde{q}(\delta_\alpha) &= Q(\alpha_0\,(1+\delta_\alpha))/m_e\,,
\end{aligned}
\tag{58}
$$

and the factor determining the variation of the β-decay rate with a variation of α, see Eq. (57), is determined by evaluating $f(\tilde{a}, \tilde{p})$ and $f(a,p)$ via Eq. (53).

We note that $Q(\alpha) = Q(\alpha_0(1+\delta_\alpha)) \geq m_e$, $Q(\alpha_0) \geq m_e$ implies an upper limit for δ_α :

$$(V_a^C - V_c^C \mp \Delta m_{\rm QED})\,\delta_\alpha \geq m_e - Q(\alpha_0) \\ \Leftrightarrow \delta_\alpha \leq \frac{Q(\alpha_0) - m_e}{V_c^C - V_a^C \pm \Delta m_{\rm QED}} \,. \tag{59}$$

As for other cases where during a variation of α the Q-value of a reaction becomes negative, we have put the corresponding rate to zero.

We also note that for the neutron decay $n \to p + e^- + \overline{\nu}$ the variation of the rate with a variation of α merely implies a variation of the neutron lifetime $\tau_n \propto 1/\lambda_{n\to p}$.

2.5.3 *Implications for the weak $n \leftrightarrow p$ reactions*

As detailed in Ref. [26] the six reactions

$$\begin{aligned} &n + \nu \leftrightarrow p + e^- \,, \\ &n \leftrightarrow p + e^- + \overline{\nu} \,, \\ &n + e^+ \leftrightarrow p + \overline{\nu} \,, \end{aligned} \tag{60}$$

determine the evolution of the neutron abundance in the early phase of BBN and hence are crucial for all other primordial nuclear abundances. Assuming local thermodynamical equilibrium in terms of a temperature T and a distinct neutrino temperature T_ν in the so-called infinite nucleon mass approximation the $n \to p$ (angular averaged) reaction rate can be written, see *e.g.* [26] for details, as

$$\begin{aligned} \Gamma_{n\to p}(\Delta m; T) &= \Gamma_{\substack{n+\nu\to p+e^- \\ n\to p+e^-+\overline{\nu}}} + \Gamma_{n+e^+\to p+\overline{\nu}} \\ &= K \int_{m_e}^{\infty} {\rm d}E \; E\sqrt{E^2 - m_e^2} \\ &\quad \times \Bigg[(E+\Delta m)^2 \, g\left(\frac{E+\Delta m}{k_B T_\nu}\right) g\left(-\frac{E}{k_B T}\right) \\ &\quad + (-E+\Delta m)^2 \, g\left(\frac{-E+\Delta m}{k_B T_\nu}\right) g\left(\frac{E}{k_B T}\right) \Bigg] \end{aligned} \tag{61}$$

with

$$g(x) = \frac{1}{{\rm e}^x + 1} \tag{62}$$

the Fermi-Dirac distribution function. The ratio T_ν/T follows from the cosmological evolution, see the black curve in Fig. 2.

The constant K is fixed by requiring that $\Gamma_{n\to p}(\Delta m; 0) = 1/\tau_n$, with τ_n the neutron lifetime. The $p \to n$ rate is simply given by substituting $\Delta m \mapsto -\Delta m$ in Eq. (61) above. In this case $\Gamma_{p\to n}(\Delta m; 0) = 0$. As discussed in [26] and [31] there are a number of corrections to the $n \to p$ and $p \to n$ rates as given above, *viz.* the Coulomb correction

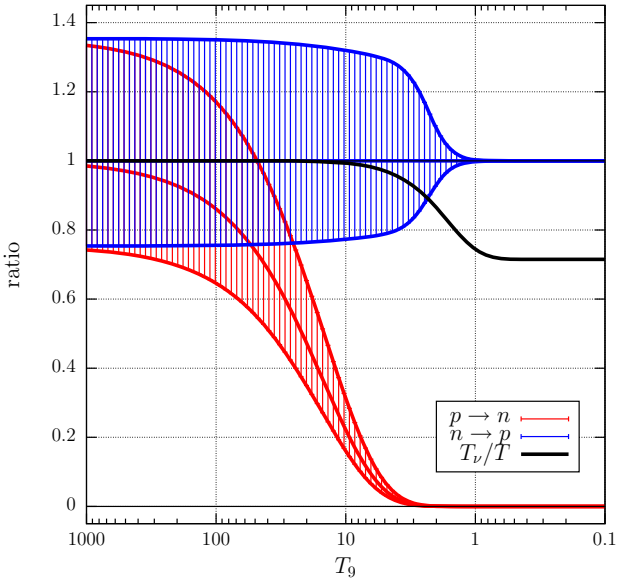

Fig. 2 Variation of the rate ratios $R_{n\to p}$ (Eq. (63), blue hatched area) and $R_{p\to n}$ (Eq. (64), red hatched area) with decreasing temperature ($T_9 = T/[10^9\,{\rm K}]$) for δ_α in the range $\delta_\alpha = -0.1$ (lower curves) up to $\delta_\alpha = 0.1$ (upper curves). Also shown is the ratio T_ν/T (black curve)

(as discussed above in Sect. 2.5.2), electromagnetic radiative corrections, finite nucleon mass corrections, plasma corrections and non-instantaneous neutrino decoupling effects. Some of these involve the fine-structure constant α, but since these effects are small corrections anyway, the most relevant effect when varying α is through the change $\Delta m(\alpha) = \Delta m(\alpha_0) - \Delta m_{\rm QED}\,\delta_\alpha$. This effect is illustrated in Fig. 2, where the double rate ratios

$$R_{n\to p} = \frac{\Gamma_{n\to p}(\Delta m(\alpha); T)\,\Gamma_{n\to p}(\Delta m(\alpha_0); 0)}{\Gamma_{n\to p}(\Delta m(\alpha); 0)\,\Gamma_{n\to p}(\Delta m(\alpha_0); T)} \,, \tag{63}$$

and

$$R_{p\to n} = \frac{\Gamma_{p\to n}(\Delta m(\alpha); T)\,\Gamma_{n\to p}(\Delta m(\alpha_0); 0)}{\Gamma_{n\to p}(\Delta m(\alpha); 0)\,\Gamma_{n\to p}(\Delta m(\alpha_0); T)} \,, \tag{64}$$

obtained by a numerical integration according to Eq. (61) (with a method similar to that of Eq. (4)) are plotted as a function of $T_9 = T/[10^9\,{\rm K}]$). This double ratio was chosen such that for $T \to 0$ the $n \to p$ curves tend to unity and the $p \to n$ curves to zero; the α-dependence of the $n \to p$ rate in this low-temperature limit is then given by the expressions in the preceding Sect. 2.5.2. As is evident from this figure the variation of the rates with varying α is non-linear and strongly temperature dependent.

2.6 The $n + p \to d + \gamma$ reaction

Fortunately, for the $n + p \to d + \gamma$ reaction an accurate treatment within the framework of pionless EFT [38,39] is available. Accordingly, for this leading nuclear reaction in

the BBN network it is possible to study dependences of the cross section and hence of the reaction rate on various nuclear parameters, such as the binding energy of the deuteron, np scattering lengths, effective ranges *etc.* as was done in [19]. Here we shall focus on the α-dependence.

The cross section was given in [39] as

$$\begin{aligned}\sigma_{np\to d\gamma}(p) &= 4\pi\,\alpha \\ &\times\left(1-\frac{2\,p^4+4\,p^2\,\gamma^2+3\,\gamma^4}{4\,m_N^2\,(p^2+\gamma^2)}\right)\frac{(\gamma^2+p^2)^3}{\gamma^3\,m_N^4\,p} \\ &\times\left[\left\langle\widetilde{\chi}_{E1_V}\right\rangle^2+\left\langle\widetilde{\chi}_{M1_V}\right\rangle^2+\left\langle\widetilde{\chi}_{M1_S}\right\rangle^2+\left\langle\widetilde{\chi}_{E2_S}\right\rangle^2\right], \end{aligned} \tag{65}$$

where p is the relative momentum, $m_N = (m_p + m_n)/2$ denotes the nucleon mass, $\gamma = \sqrt{B_d\,m_N}$ is the so-called binding momentum, with $B_d = 2.225$ MeV the binding energy of the deuteron, and $\left\langle\widetilde{\chi}_{E1_V}\right\rangle^2$, $\left\langle\widetilde{\chi}_{M1_V}\right\rangle^2$, $\left\langle\widetilde{\chi}_{M1_S}\right\rangle^2$, $\left\langle\widetilde{\chi}_{E2_S}\right\rangle^2$, are the dimensionless amplitudes for isovector electric dipole, isovector magnetic dipole, isoscalar magnetic dipole and isoscalar electric quadrupole contributions, respectively. For the energies relevant in BBN only the isovector contributions are significant and these were calculated at N4LO and N2LO for the electric and magnetic parts, respectively. The overall theoretical uncertainty is claimed to be better than 1% for CMS energies $E \leq 1$ MeV. The expression of Eq. (65) with all terms included was used to calculate the cross section for this reaction throughout the present investigation.

Concerning the variation of this cross section when varying $\alpha = \alpha_0\,(1+\delta_\alpha)$ it is evident that the dominant effect is simply

$$\sigma_{np\to d\gamma}(\alpha;\,p) = (1+\delta_\alpha)\,\sigma_{np\to d\gamma}(\alpha_0;\,p)\,. \tag{66}$$

Note that there is no Coulomb-contribution to the binding energy of the deuteron, while the expectation value $\langle v^{EM}\rangle$ of the electromagnetic interaction, mainly due to the magnetic dipole-dipole interaction moment term, see [40] for a treatment based on the Argonne v_{18} nucleon-nucleon potential, is very small, $\langle v^{EM}\rangle = 0.018$ MeV. Hence the effects of a change of the Q-value of the reaction with varying α, as discussed in the previous subsections, as well as any other electromagnetic effects on the structure of the deuteron are considered to be negligible in the present context. Moreover, in the expression of Eq.(65), as well as in the expressions for the amplitudes $\widetilde{\chi}$ of Ref. [39] the nucleon mass $m_N = (m_p + m_n)/2$ occurs at various instances. Although a moderately accurate value for the electromagnetic contribution to the neutron-proton mass difference is available (and was, in fact, used in our discussion of the β-decays in Sect. 2.5.1), only rough estimates are available for the electromagnetic contribution to the neutron and proton mass separately. In Eq. (12.3) of Ref. [42] the estimates $m_p^{\rm Born} \approx 0.63\,\text{MeV}, m_n^{\rm Born} \approx -0.13\,\text{MeV}$ (with an estimated accuracy of ≈ 0.3 MeV) for the total electromagnetic self-energy can be found, which, via $m_N^{\rm Born} \approx 0.25$ MeV, would imply that m_N varies with α (putting $m_N \approx 1$ GeV for this estimate) as

$$m_N(\alpha) \approx m_N(\alpha_0)(1 + 0.00025\,\delta_\alpha)\,. \tag{67}$$

For $|\delta_\alpha| < 0.1$, as considered here, this would lead to effects well below the theoretical accuracy quoted above and therefore this effect was neglected and the variation of the $n+p \to d+\gamma$ cross section with α is assumed to be entirely given by Eq. (66).

2.7 Coulomb energies

A variation of the value of the fine-structure constant α implies a variation of the nuclear binding energies and hence a variation of the Q-values of the reactions, which in turn leads to a variation of the cross sections and the corresponding rates. Therefore the present study requires an estimate of the electromagnetic contribution to the nuclear masses or equivalently to the nuclear binding energies. A rough estimate is provided by the Coulomb term in the Bethe-Weiszsäcker formula (for a recent determination, see *e.g.* [43] and references therein):

$$V_i^C = a_C\,\frac{Z_i\,(Z_i-1)}{A^{\frac{1}{3}}}\,, \qquad a_c \approx 0.64\,\text{MeV}\,, \tag{68}$$

approximately accounting for the Coulomb repulsion by the protons in a nucleus. However, this formula is not very precise when applied to the light nuclei relevant here. We therefore prefer to use the expectation values of the Coulomb interaction as determined from a recent *ab initio* calculation of light nuclear masses in the framework of Nuclear Lattice Effective Field Theory (NLEFT) [44], listed in Table 1. We also compare the calculated binding energies to the experimental data as used here in order to give an impression of the quality of the calculation.

3 Calculation of the reaction rates

For the 18 leading nuclear reactions in the BBN network, *viz.* the radiative capture reactions

$$\begin{array}{llll} n+p & \to d+\gamma\,, & d+p & \to {}^3\text{He}+\gamma\,, \\ p+{}^3\text{H} & \to {}^4\text{He}+\gamma & d+{}^4\text{He} & \to {}^6\text{Li}+\gamma\,, \\ p+{}^6\text{Li} & \to {}^7\text{Be}+\gamma\,, & {}^3\text{H}+{}^4\text{He} & \to {}^7\text{Li}+\gamma\,, \\ {}^3\text{He}+{}^4\text{He} & \to {}^7\text{Be}+\gamma\,, & & \end{array} \tag{69}$$

the charged particle reactions

$$\begin{array}{ll} d+d \to {}^3\text{H}+p\,, & d+d \to {}^3\text{He}+n\,, \\ d+{}^3\text{H} \to {}^4\text{He}+n\,, & d+{}^3\text{He} \to {}^4\text{He}+p\,, \\ p+{}^6\text{Li} \to {}^3\text{He}+{}^4\text{He}\,, & p+{}^7\text{Li} \to {}^4\text{He}+{}^4\text{He}\,, \\ d+{}^7\text{Li} \to {}^4\text{He}+{}^4\text{He}+n\,, & d+{}^7\text{Be} \to {}^4\text{He}+{}^4\text{He}+p\,, \end{array} \tag{70}$$

Table 1 Binding energies B (calculated (*cal*) and experimental (*exp*) values) and expectation values for the Coulomb interaction V^C of light nuclei

Nuclide	V^C [MeV][a]	B_{cal} [MeV][a]	B_{exp} [MeV][b]
^{2}H	0.0	2.215(150)	2.225
^{3}H	0.0	8.35(22)	8.482
^{3}He	0.688(1)	7.64(14)	7.718
^{4}He	0.759(0)	28.24(16)	28.296
^{6}Li	1.574(2)	32.82(12)	31.994
^{7}Li	1.599(2)	39.61(13)	39.245
^{8}Li	1.649[c]		41.278
^{7}Be	2.722[c]		37.600
^{9}Be	2.951(4)	57.59(29)	58.164
^{8}B	4.212[c]		37.737
^{10}B	4.453(8)	64.46(59)	64.750
^{11}B	4.962(2)	75.38(42)	76.204
^{12}B	4.852[c]		79.574
^{11}C	6.933[c]		73.440
^{12}C	7.144(16)	92.36(64)	92.161
^{13}C	7.151(7)	97.07(52)	97.107
^{14}C	7.317(7)	104.87(69)	105.284
^{12}N	9.483[c]		74.040
^{13}N	9.854[c]		94.104
^{14}N	10.354(4)	106.25(94)	104.657
^{15}N	10.054(2)	115.29(37)	115.491
^{14}O	12.977[c]		98.730
^{15}O	13.320[c]		111.953
^{16}O	13.412(10)	129.99(38)	127.617

[a]From [44]. The errors quoted in parentheses include all the statistic and systematic uncertainties. In case of ^{2}H, the error is entirely given by the variation of the np phase shifts at N3LO within their uncertainties
[b]From [45], as used in the present work
[c]Extrapolated from a least-squares fit to the other data with $V^C(N,Z) = \sum_{k=0}^{2}\sum_{l=0}^{1} c_{kl}(N-Z)^l(N+Z)^k$. where $c_{00} = 0.653$, $c_{10} = -0.232$, $c_{20} = 0.065$, $c_{01} = 0.060$, $c_{11} = -0.060$, $c_{21} = -0.003$ [in MeV]

and the neutron-induced reactions

$$n+{}^{3}\mathrm{He}\to{}^{3}\mathrm{H}+p\,,\qquad n+{}^{7}\mathrm{Be}\to{}^{7}\mathrm{Li}+p\,,\qquad n+{}^{7}\mathrm{Be}\to{}^{4}\mathrm{He}+{}^{4}\mathrm{He}\,, \tag{71}$$

the rates and their variations with α are calculated by a numerical integration of Eq. (38) and tabulated for 60 temperatures in the range $0.001 \le T_9 = T/[10^9\ \mathrm{K}] \le 10.0$. These values were then used via a cubic spline interpolation in the four publicly available BBN codes as outlined in Sect. 4. The resulting rates and their variations with $\alpha = \alpha_0\,(1+\delta_\alpha)$ in the range $\delta_\alpha \in [-0.1, 0.1]$ are displayed in Fig. 1 in Sect. 2.4. To this end, we made new fits to the cross sections (or equivalently of the corresponding astrophysical S-factors) for the reactions listed above. The parameterizations can be found in Appendix A. In addition in Fig. 3 the resulting reaction rates for $\alpha = \alpha_0$ are compared to the rates implemented in the original versions of the four programmes considered here.

In Fig. 3 we also display the rates obtained with the NACRE II database, see [46], which served as a further check on our calculated reaction rates at $\alpha = \alpha_0$. The rates of all other reactions were taken as in the original implementation of the codes and the variation of the rates with α was calculated as discussed in Sect. 2.4.

The variation of the β-decay rates according to Eq. (57) was implemented directly in the various codes. In Fig. 4 it is shown how the β-rates at low temperature (*i.e.* $T \ll T_9$) change by a variation of $\alpha = \alpha_0\,(1+\delta_\alpha)$. In particular the rates of the tritium decay and the ^{14}C-decay strongly depend on the value of δ_α, the effect of (relatively large) changes in the (relatively small) Q-values due to changes in the Coulomb contribution to the binding energies being dominant.

As already touched upon in Sect. 2.5.3 the variation of the weak $n \leftrightarrow p$ rates with α is dominated by the variation of proton-neutron mass difference with α and is strongly temperature dependent in the early phase of BBN. In the default version of the Kawano code `NUC123` [20] this temperature dependence is parametrized as outlined in Appendix F of Ref. [20], but a numerical integration along Eq. (61) can be enforced and was in fact used to implement the α-dependence of these rates. The `PArthENoPE` code [23–25] contains a slightly more sophisticated parameterization, see *e.g.* Appendix C of Ref. [31], accounting also for some higher order corrections. Here we used the α-dependence of the $n \leftrightarrow p$ rates as illustrated in Fig. 2 as a factor multiplying the parametrized rate. In the `AlterBBN` code [21,22] the temperature dependence of the weak $n \leftrightarrow p$ rates was already determined numerically as in Eq. (61) and the α dependence can be accounted for by an appropriate variation of Δm. In this code also the Coulomb correction, see Eq. (57), was included in the integrand of Eq. (61), but this was found to have no significant impact on the final abundances to be discussed below in Sect. 5. The `PRIMAT` [26] implementation offers the possibility to study the α-dependence of the weak $n \leftrightarrow p$ reactions in all detail including all the higher order electromagnetic corrections mentioned in Sect. 2.5.3. In fact this code was used to verify that the variation of the rates through the variation of Δm with α as discussed in Sect. 2.5.3 is indeed the dominant effect. Indeed, ignoring the α dependence in the higher order corrections implemented in `PRIMAT` led to response coefficients that differ at most by 0.5% from the values listed in Table 3 below. Accordingly, in spite of the fact that the $n \leftrightarrow p$ reactions are treated at various levels of sophistication, the resulting primordial abundances and their variation with α, to be discussed in Sect. 5, were found to be rather consistent.

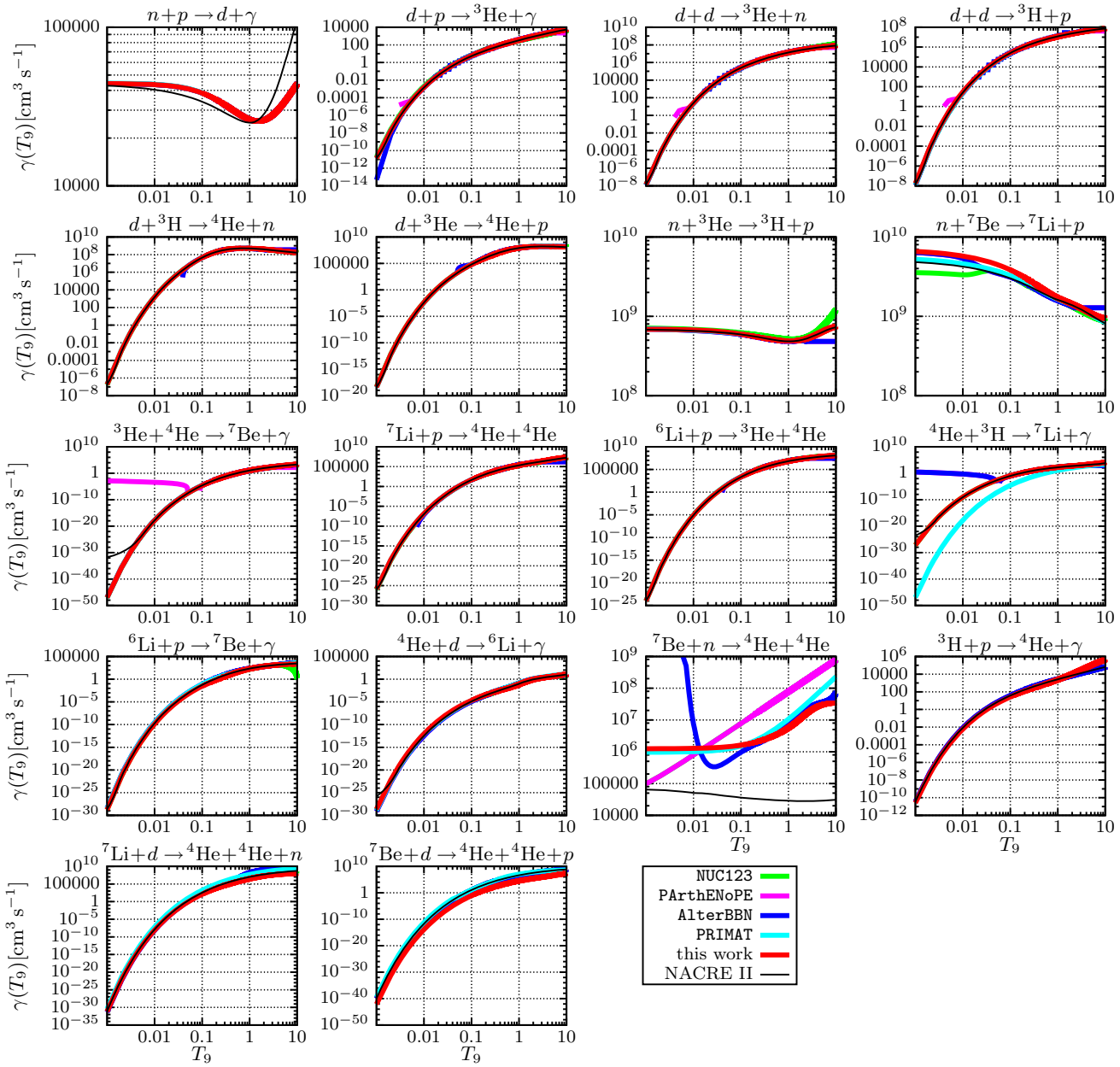

Fig. 3 Reaction rates $\gamma(T_9)$ for 18 leading nuclear reactions in the BBN network, where $T_9 = T/[10^9\ \mathrm{K}]$. The rates resulting from the new parameterizations of the S-factors in Appendix A are represented by solid red curves (color online). The rates in the original version of the programmes are given by green curves for `NUC123` [20], magenta curves for `PArthENoPE` [25], blue curves for `AlterBBN` [22] and cyan curves for the `PRIMAT` [26] code. Also shown as a thin black curve is the result from the NACRE II database, see [46]

4 The BBN response matrix

We estimated the linear dependence of the primordial abundances Y_n on small changes in the value of the fine-structure constant $\alpha = \alpha_0\,(1+\delta_\alpha)$ by calculating the abundance of the nuclide n, with

$$n \in \{{}^2\mathrm{H}\,,\,{}^3\mathrm{H}+{}^3\mathrm{He}\,,\,{}^4\mathrm{He}\,,\,{}^6\mathrm{Li}\,,\,{}^7\mathrm{Li}+{}^7\mathrm{Be}\} \tag{72}$$

i.e. $Y_n(\alpha_0\,(1+\delta_\alpha))$, for fractional changes δ_α in the range $[-0.1, 0.1]$ with the publicly available codes for BBN, namely a version of the Kawano code `NUC123` [20] (in `FORTRAN`), two more modern implementations based on this, namely `PArthENoPE` [23–25] (`in FORTRAN`) and `AlterBBN` [21,22] (in `C`) as well as an implementation as a `mathematica`-notebook, `PRIMAT` [26]. To this end we performed least-squares fits of a quadratic polynomial to the abundances:

$$P_k(\delta_\alpha) = c_0\left(1 + c_1\,\delta_\alpha + c_2\,\delta_\alpha^2\right)\,, \tag{73}$$

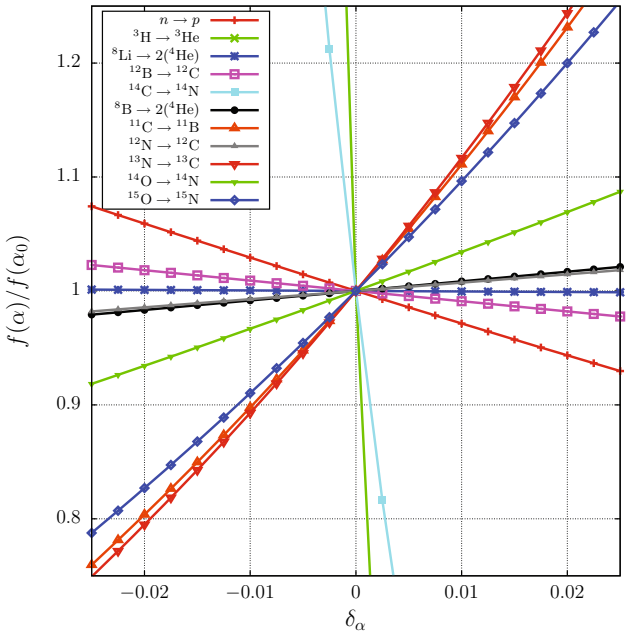

Fig. 4 Fractional variation of the β-rates at low temperature with $f(\alpha)/f(\alpha_0)$ calculated by Eq. (57)

such that

$$\frac{\partial}{\partial c_j} |Y_n/Y_H(\alpha_0\,(1+\delta_\alpha)) - P_k(\delta_\alpha)|^2 = 0\,, \quad j = 0, 1, 2\,. \tag{74}$$

Then

$$\frac{\partial \log\,(Y_n/Y_H)}{\partial \log \alpha} \approx c_1 \tag{75}$$

will be called an element of the linear nuclear BBN response matrix. It represents the dimensionless fractional change in the primordial abundance ratio Y_n/Y_H due to a fractional change α in linear approximation. Deviations from a linear response are then given by the coefficient c_2.

5 Results and discussion

In most of what follows we shall use $\eta = 6.14 \cdot 10^{-10}$ from Ref. [30] as the nominal baryon-to-photon density ratio while varying α. The programs were modified as indicated in Sect. 4 of Ref. [19] and the rates for the most relevant reactions listed in Sect. 3, resulting from the new fits of the cross sections presented in Appendix A, were used in all programmes.

The resulting nominal (*i.e.* at $\alpha = \alpha_0$) abundances at the end of the BBN epoch in terms of the number ratios $Y_{^2\mathrm{H}}/Y_\mathrm{H}$, $Y_{^3\mathrm{H}+^3\mathrm{He}}/Y_\mathrm{H}$, $Y_{^6\mathrm{Li}}/Y_\mathrm{H}$, $Y_{^7\mathrm{Li}+^7\mathrm{Be}}/Y_\mathrm{H}$, and the mass ratio for ^{4}He are compared to the values quoted in Ref. [19] and experimental data in Table 2. Although the mass ratio for ^{4}He and, to a minor extend, the number ratio for deuterium did not change significantly with respect to the values obtained in Ref [19], the $^3\mathrm{H} + {}^3\mathrm{He}$ number ratio increased by approximately 10% and the ^{6}Li number ratio was found to be larger by about 60–80%. The latter increase was found to be mainly due to the new parameterizations of reactions involving ^{6}Li. In particular, substituting the original parameterization of the S-factor for the $d + {}^4\mathrm{He} \to {}^6\mathrm{Li} + \gamma$ reaction, see Eq. (A6) and Fig. 15, for this reaction alone already increases the number ratio for ^{6}Li to $\approx 1.7 \times 10^{-14}$. Furthermore, the $^7\mathrm{Li} + {}^7\mathrm{Be}$ number ratio is still too large by a factor of three, a phenomenon known as the lithium-problem, which is thus unsolved even with the updated cross sections used here. As stated previously in [19], in spite of this unresolved issue in BBN the consistency of the cosmic microwave background observations with the determined abundances of deuterium and helium is considered to be a non-trivial success. Accordingly, we think that this issue is no obstacle for the study presented here.

The elements of the response matrix were then determined by a polynomial fit, as explained above in Sect. 4 for the abundances relative to the hydrogen abundance, namely $Y_{^2\mathrm{H}}/Y_\mathrm{H}$, $Y_{^3\mathrm{H}+^3\mathrm{He}}/Y_\mathrm{H}$, $Y_{^6\mathrm{Li}}/Y_\mathrm{H}$, $Y_{^7\mathrm{Li}+^7\mathrm{Be}}/Y_\mathrm{H}$, and the mass ratio for ^{4}He.

The dependence of these ratios on the value of the fine structure constant $\alpha = \alpha_0\,(1 + \delta_\alpha)$ is displayed in Fig. 5 for $\delta_\alpha \in [-0.1, 0.1]$.

Indeed the variation of the abundance ratios is found to be very similar for all four publicly available codes, in spite of the fact that these codes differ in details, such as the number of reactions in the BBN network or the manner in which the rate equations are solved numerically. Note, however, that in the present study the rates calculated for the major reactions listed in Sect. 3 and their variation with α are the same.

Of course this then also applies to the values for the resulting response matrix elements. The response matrix elements $\partial\,\log\,(Y_n/Y_H)/\partial\,\log\,\alpha = c_1$ and the coefficients of the quadratic term in Eq. (73) are given and compared to some results from the literature in Table 3. Note that with the exception of ^{6}Li, we have $|c_2| \simeq |c_1|$, so that due to the smallness of α, the second order contribution to the response is of minor importance. All programs were run with the full network implemented in the original version codes. We checked that if we run the programs with a smaller network the results listed in Tables 2,3 change only in the last digit and therefore conclude that the approximation, see Sect. 2.4, we made for rate changes in the reactions beyond the reactions listed in Eqs. (69–71) are without any effect for the present investigation.

Apart from the values of c_1 for $^2\mathrm{H}(\approx 3.6)$ and for $^6\mathrm{Li}(\approx 6.8)$ the values obtained in the present study, although consistent among each other, differ appreciably from the values obtained in Refs. [7,8,10]. In particular in the present calculations the linear response for $^3\mathrm{H} + {}^3\mathrm{He}$ is much larger while the linear response for $^7\mathrm{Li} + {}^7\mathrm{Be}$ is appreciably smaller

Table 2 Final abundances as number ratios Y_n/Y_H (for ^{4}He the mass ratio Y_p) calculated with the modified versions of the codes. The value of the baryon-to-photon ratio and the nominal value of the neutron lifetime are $\eta = 6.14 \cdot 10^{-10}$ and $\tau_n = 879.4$ s, respectively. For comparison also the values previously obtained in Ref. [19] are listed

Code	^{2}H $\times 10^5$	^{3}H+^{3}He $\times 10^5$	Y_p	^{6}Li $\times 10^{14}$	^{7}Li+^{7}Be $\times 10^{10}$
NUC123	2.501	1.139	0.246	1.809	5.172
[19]	2.550	1.040	0.247	1.101	4.577
PArthENoPE	2.569	1.147	0.247	1.820	5.017
[19]	2.511	1.032	0.247	1.091	4.672
AlterBBN	2.585	1.153	0.248	1.904	4.993
[19]	2.445	1.031	0.247	1.078	5.425
PRIMAT	2.563	1.149	0.247	1.862	5.033
[19]	2.471	1.044	0.247	1.198	5.413
PDG [30]	2.547		0.245		1.6
±	0.025		0.003		0.3

in magnitude, although there seems to be at least a consensus concerning the sign.

In order to clarify this issue, we shall discuss in some detail the relevance of the various factors that reflect the α-dependence of the nuclear rates:

- First of all we list in Table 4 the linear response of the BBN abundances to a variation of α in the β-decay rates only.
- In Table 5 we display the linear response of the BBN abundances to a variation of the nuclear reaction rates. The relevance of the variation of the binding energies with α may be appreciated by the linear response due to changes in α accounting for the effects due to the Coulomb penetration factors only, *i.e.* without accounting for changes in the binding energies, listed in Table 6. Here we also compared our results to the results presented in Table I of Ref. [10] for the dependence of the abundances on the nuclear rate variation with α, that thus differ from our results significantly for $c_1(^3\mathrm{H}+^3\mathrm{He})$ and $c_1(^7\mathrm{Li}+^7\mathrm{Be})$, our results being larger in magnitude for the former and smaller for the latter.

^{2}H	^{3}H + ^{3}He	Y_p	^{6}Li	^{7}Li + ^{7}Be
3.7	3.5	1.4	7.0	− 4.4

Indeed, if we substitute our values, as well as the results we obtained in [19] for the linear response of the abundances on binding energies and the neutron life-time τ_n for the values of the response matrix C of Table I in [10] and furthermore account for the smaller value $\partial \log \tau_n/\partial \log \alpha \approx 2.90$, obtained via Eq. (57) (instead of 3.86 in [10]) and the smaller value $\partial \log Q_N/\partial \log \alpha \approx$-0.45 (instead of -0.59 in [10]), due to the smaller new value for Δm_{QED}, and use our values for the response of the binding energies $\partial \log B_i/\partial \log \alpha$ that are smaller by about 10% in Table IV of [10] we find approximately for the linear responses

rather close to our values for c_1 given in Table 3. Most of the effects listed above are, although significant, of minor importance only, and accordingly the difference can be traced back to the fact that our results for the variation of the rates with a variation of α when ignoring the effects based on Q-value changes, as listed in Table 6 differ appreciably from those of [10]. Unfortunately in the latter reference no results on the α-dependence of the rates are explicitly given. In appendix A.2 of [10] it is mentioned that parameterizations of the S-factors were used, the parameters determined by fitting the NETGEN rates as closely as possible. In order to check our parameterizations of the nuclear rates we compared our rates with results generated by the NETGEN-tool [46] in Fig. 3 and found that these are indeed compatible for all reactions, except for the reaction $^7\mathrm{Be} + n \rightarrow {}^4\mathrm{He} + {}^4\mathrm{He}$, where the NETGEN-tool merely uses the THALYS nuclear reaction model [47]. We instead used data, see also Fig. 26 for our fit of the S-factor. Therefore the difference must be due to the different way the Coulomb penetration effects are treated. Note that, as emphasized in Sect. 2.1.1, we did not rely on temperature-independent penetration factors taken as a Gamow-factor, but rather accounted for the penetration dependences in the cross-section, which then leads to temperature-dependent changes in the rates.

Our results also differ from the results in Refs. [8] and [7] published even earlier. Concerning the treatment in [8], it is noted that, although the authors present a detailed discussion of the α-dependence in the penetration factors, even accounting for additional α-dependent effects due to the peripheral nature of some radiative capture reactions such as *e.g.* the $^3\mathrm{He} + {}^4\mathrm{He} \rightarrow {}^7\mathrm{Be} + \gamma$, an effect taken into account also in the present treatment. Nevertheless, in contrast to our treatment, α-dependent effects seem to be treated merely

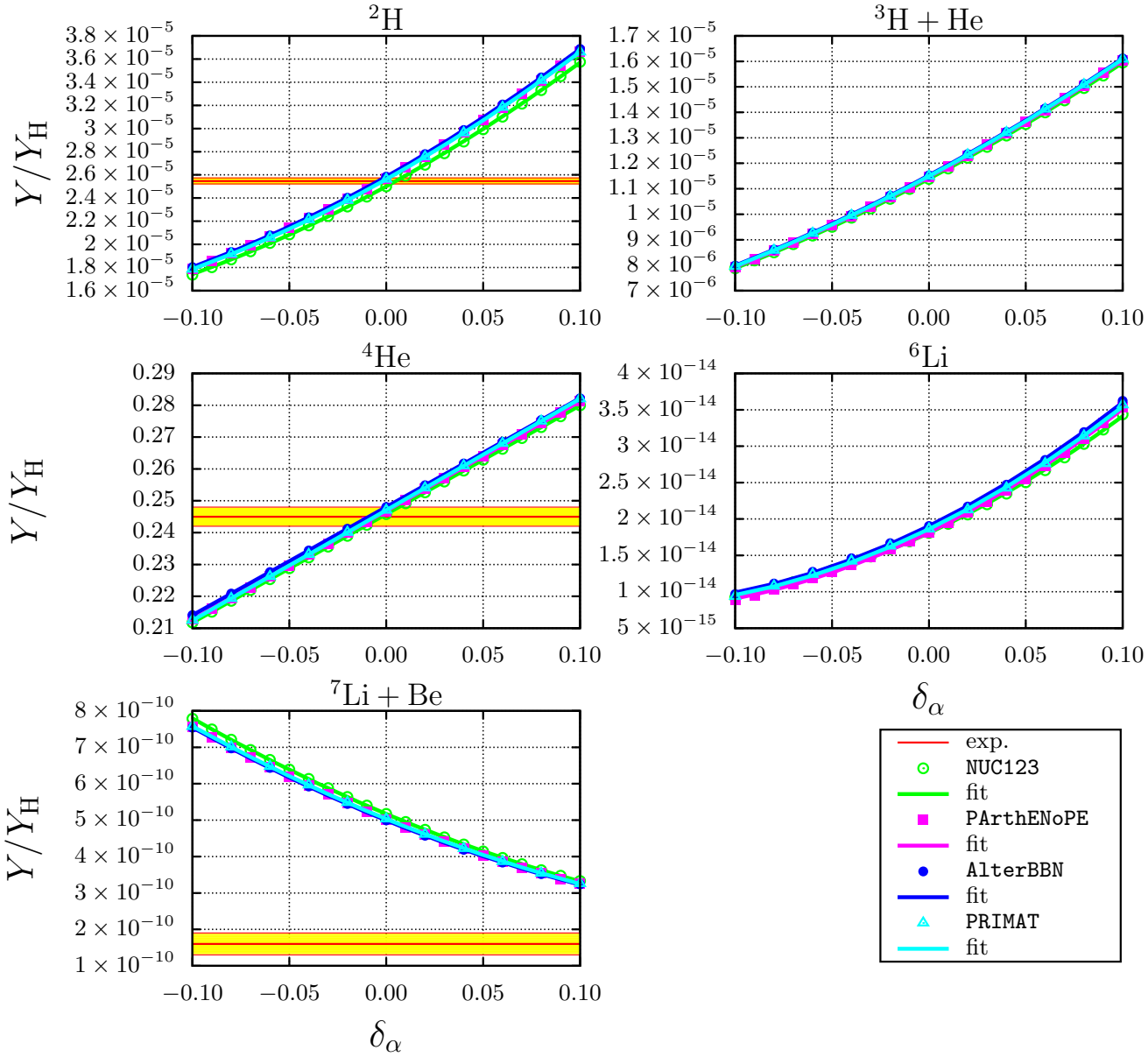

Fig. 5 Variation of the abundance ratios Y_n/Y_H with a variation of $\alpha = \alpha_0\,(1+\delta_\alpha)$ for $\delta_\alpha \in [-0.1, 0.1]$ obtained with the codes: `NUC123` [20], `AlterBBN` [22], `PArthENoPE` [25], `PRIMAT` [26]. Here, we use $\eta = 6.14 \cdot 10^{-10}$ and $\tau_n = 879.4$ s. Also shown are the solid curves obtained by the fits according to Eq. (73) with the parameters listed in Table 7. The experimental values cited in PDG [30] (thick red lines) are indicated by yellow-highlighted regions (color online) representing the 1σ limits by red lines

by temperature-independent factors multiplying the rates. In Ref. [7], the changes in the reaction rates due to changes in α were treated through approximate expressions based on expansions of the S-factors, whereas we preferred to make no further approximations beyond the modeling of the penetration factors discussed in Sect. 2.1.1. Note that a comparison with the work of [9] is not possible, since there any variation of the fine-structure constant is tied to the variation of certain Yukawa couplings.

All in all our results indicate that the BBN abundance for ^{7}Li + ^{7}Be is less sensitive and the abundance of ^{3}H + ^{3}He is more sensitive to variations of the value of the electromagnetic fine-structure constant α than what was determined earlier. Note that such a reduced sensitivity on nuclear quantities, such as binding energies *etc.* was also observed in [19]. There it was also found that this is mainly due to inclusion of the temperature-dependent changes in the rates. Unfortunately, the primordial abundance of ^{3}H + ^{3}He is not known precisely enough to lead to any implications and the nominal prediction for the ^{7}Li + ^{7}Be abundance is too large anyway.

If we focus on the deuterium and ^{4}He abundance ratios alone we can extract from the observationally based data

Table 3 BBN response matrix $c_1 = \partial \log(Y_n/Y_H)/\partial \log \alpha$ and the coefficients c_2 of the quadratic term in Eq. (73) at $\eta = 6.14 \cdot 10^{-10}$ and $\tau_n = 879.4\,\mathrm{s}$. Y_n/Y_H are the number ratios of the abundances relative to hydrogen; Y_p is conventionally the ^{4}He/H mass ratio. The results obtained with the four BBN codes NUC123 [20], PArthENoPE [25], AlterBBN [22], PRIMAT [26] are given in four subsequent rows and compared to earlier results from Refs. [7,8,10]

Code	^{2}H		^{3}H+^{3}He		Y_p		^{6}Li		^{7}Li+^{7}Be	
	c_1	c_2	c_1	c_2	c_1	c_2	c_1	c_2	c_1	c_2
NUC123	3.655	6.228	3.540	4.625	1.387	0.016	6.830	20.412	− 4.325	7.480
PArthENoPE	3.635	6.182	3.533	4.577	1.389	0.065	7.159	21.482	− 4.308	7.715
AlterBBN	3.644	6.188	3.526	4.568	1.373	0.049	6.857	20.499	− 4.322	7.865
PRIMAT	3.658	6.264	3.534	4.595	1.408	0.081	6.953	20.828	− 4.302	7.563
[10]	3.6		0.95		1.9		6.6		− 11	
[8][a]	3.99	5.99	1.04	− 2.67					− 9.30	25.7
[7][b]	5.13	9.91	0.78	− 1.96	1.96	− 0.73			− 13.6	83.1

[a]Extracted from Fig.2 of [8] for $\eta = 5.6 \cdot 10^{-10}$ after digitizing the data
[b]Extracted from Fig.4 of [7] for $\eta = 5 \cdot 10^{-10}$ after digitizing the data

Table 4 BBN response matrix $c_1 = \partial \log(Y_n/Y_H)/\partial \log \alpha$ accounting for the variation of the β-decay rates only. See also the caption of Table 3

Code	^{2}H	^{3}H + ^{3}He	Y_p	^{6}Li	^{7}Li + ^{7}Be
NUC123	0.827	0.250	1.403	2.651	0.475
PArthENoPE	0.832	0.255	1.406	2.663	0.479
AlterBBN	0.829	0.255	1.390	2.632	0.462
PRIMAT	0.845	0.260	1.425	2.701	0.483

Table 5 BBN response matrix $c_1 = \partial \log(Y_n/Y_H)/\partial \log \alpha$ accounting for the variation of the nuclear rates only, but also including the variation of the binding energies and thus of the Q-values of the reactions. See also the caption of Table 3

Code	^{2}H	^{3}H + ^{3}He	Y_p	^{6}Li	^{7}Li + ^{7}Be
NUC123	2.818	3.271	− 0.017	4.005	− 5.192
PArthENoPE	2.795	3.261	− 0.017	4.315	− 5.152
AlterBBN	2.806	3.254	− 0.017	4.037	− 5.153
PRIMAT	2.803	3.257	− 0.017	4.059	− 5.164

Table 6 BBN response matrix $c_1 = \partial \log(Y_n/Y_H)/\partial \log \alpha$ accounting for the variation of the nuclear rates only, but excluding the variation of the binding energies. Also see caption to Table 3

Code	^{2}H	^{3}H + ^{3}He	Y_p	^{6}Li	^{7}Li + ^{7}Be
NUC123	2.619	3.559	− 0.016	5.561	− 2.059
PArthENoPE	2.599	3.550	− 0.017	5.866	− 2.005
AlterBBN	2.598	3.557	− 0.016	5.585	− 1.758
PRIMAT	2.595	3.562	− 0.017	5.610	− 1.769
[10]	2.3	0.79	0.00	4.6	− 8.1

bounds on the variation δ_α of the value of the fine-structure constant as listed in Table 7 for the four programs considered here, showing that one can allow for a variation of the fine-structure constant α by less than 2% on the basis of the results obtained with all programs considered here using the current value for the baryon-to-photon ratio $\eta = 6.14 \cdot 10^{-10}$, given in [30]. The values for the ^{4}He mass ratio Y_p obtained with all four programs are rather consistent and the range $[-0.018, 0.006]$ which is more restrictive than the rough estimate $|\delta_\alpha| < 0.1$ quoted in [7,8] and the limit $|\delta_\alpha| \leq 0.019$ mentioned in [10]. The values found on the basis of the deuterium number ratio show a larger spread, mainly because the nominal values, see Table 2, vary more strongly for the four programs. In spite of this we can determine the range $[-0.007, 0.008]$, also still more restrictive than the (1σ) range $[-0.04, 0.10]$ of [8]. Our new restrictions on the vari-

Table 7 Lower ($\delta_\alpha^{\min}$) and upper ($\delta_\alpha^{\max}$) limits for the variation δ_α of the fine-structure constant $\alpha = \alpha_0\,(1+\delta_\alpha)$ determined such that the resulting abundance lies within the error bounds of the observationally based abundance ratios for ^{2}H and ^{4}He given in [30]

Code	^{2}H		Y_p	
	$\delta_\alpha^{\min}$	$\delta_\alpha^{\max}$	$\delta_\alpha^{\min}$	$\delta_\alpha^{\max}$
NUC123	0.002	0.008	− 0.011	0.006
PArthENoPE	− 0.005	0.000	− 0.014	0.003
AlterBBN	− 0.007	− 0.001	− 0.018	0.000
PRIMAT	− 0.004	0.001	− 0.015	0.003

ation of α are also stronger than found earlier in the NLEFT analysis of the triple-alpha process in hot, old stars [48,49].

From a comparison of Tables 4, 5 and 6 we also see that the linear response for Y_p due to variations in the β-decay is the dominant effect. Indeed, as argued in [7], the variation of Y_p with α mainly depends on the variation of the proton–neutron mass difference with α , *i.e.* on $\delta m_{\rm QED}$ that enters the $n \to p$ weak decay.

As was done previously in Ref. [8] we also studied to what extend the results presently obtained vary with variations of the baryon-to-photon ratio η and found that our results for the linear response coefficients c_1 do not change significantly if η is varied within the error range quoted in [30], $\eta_{10} = \eta \cdot 10^{10} = 6.143 \pm 0.190$. With the values of the primordial abundance ratios for d, ^{4}He and ^{7}Li+^{7}Be mentioned in PDG [30] we can derive parameter ranges for restricting δ_α and η as presented in Figs. 6, 7, and 8. Note that we here allowed for a variation of η well beyond the currently accepted limits quoted in [30]. The results are similar to those obtained in Ref. [8] although the regions of possible values for the δ_α- and η-values are narrower here due to the newer, more precise observational data quoted in [30]. The comparison of these results again show that the value of the Li/Be abundance is incompatible with the other data and we therefore refrain from any conclusions concerning possible variations of α on the basis of the ^{7}Li observation.

We close this section with the remark that we also examined whether the use of a much smaller network, *e.g.* considering, apart from the weak reactions only 12 nuclear reactions instead of the more than 400 reactions implemented in PRIMAT would affect our conclusions significantly. It was found that the differences in the results were much smaller than the variation between the four codes considered. Nevertheless we preferred to quote results only for the full nuclear reaction networks as implemented in the four codes.

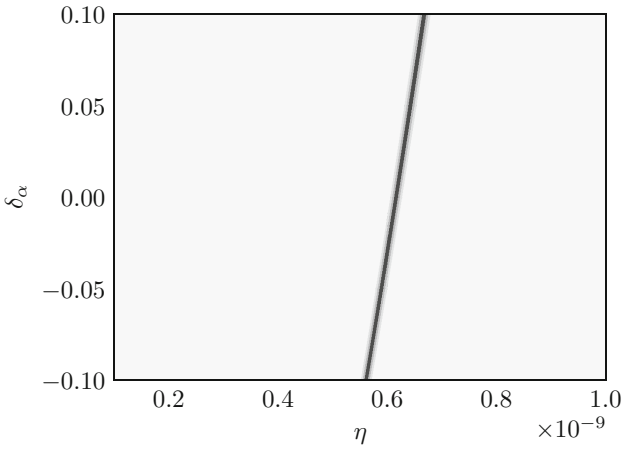

Fig. 6 Restriction on the parameters δ_α and η based on the experimental value of $Y_{^2\mathrm{H}}/Y_H$ from [30]. Shown are the corresponding 1σ (black), 2σ (dark gray) and 3σ (light gray) regions

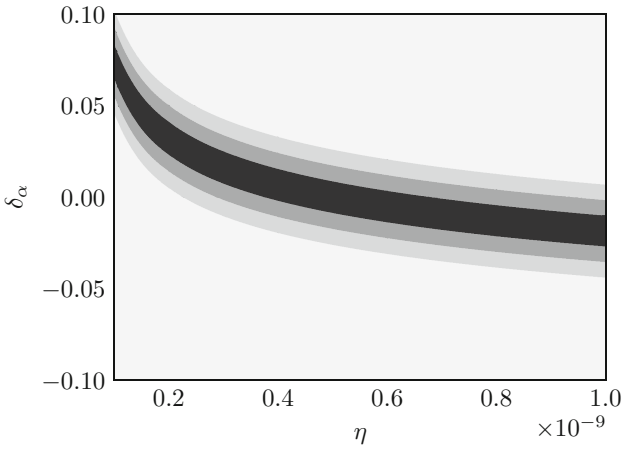

Fig. 7 Restriction on the parameters δ_α and η based on the experimental value of Y_p from [30]. Shown are the corresponding 1σ (black), 2σ (dark gray) and 3σ (light gray) regions

6 Summary

In the present paper we investigated the impact of variations in the value of the fine-structure constant α on the abundances of the light elements, *viz.* ^{2}H, ^{3}H + ^{3}He, ^{4}He, ^{6}Li and ^{7}Li + ^{7}B in primordial nucleosynthesis (BBN), keeping all other fundamental parameters fixed on their values obtained in our universe. In order to estimate possible model dependences concerning *e.g.* the number of reactions in the BBN nuclear network, the parameterizations of the nuclear rates or the manner in which the corresponding rate equations

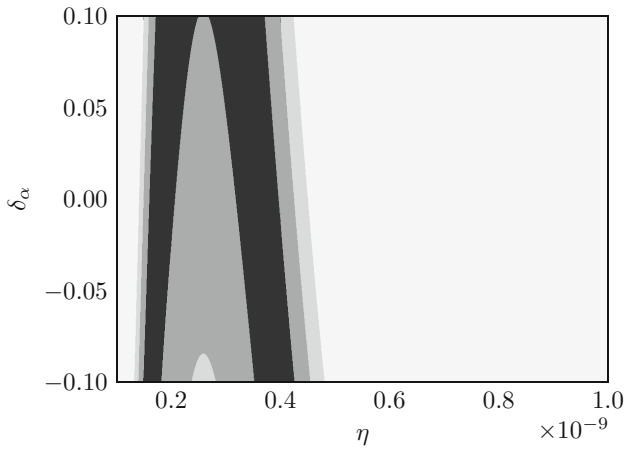

Fig. 8 Restriction on the parameters δ_α and η based on the experimental value of $Y_{(^7\mathrm{Li}+^7\mathrm{Be})}/Y_H$ from [30]. Shown are the corresponding 1σ (black), 2σ (dark gray) and 3σ (light gray) regions

are numerically solved, we compared the results obtained by using four different publicly available codes. Ideally such an investigation requires an accurate *ab initio* theory of nuclear reactions accounting for all possible electromagnetic effects. Unfortunately, however, for reactions involving the strong nuclear interaction this is only realized for the leading nuclear reaction in the BBN network, the $n + p \to d + \gamma$ reaction in the framework of pionless EFT. For all other reactions of this kind we rely on modifications of experimentally determined reaction cross sections, trying to account for electromagnetic effects, such as penetration factors, modeling the suppression due to the Coulomb barrier in channels involving charged particles as well as changes in the binding energies of nuclides due to the Coulomb repulsion of the protons and hence the Q-values of the nuclear reactions where these are involved. To this end we made new parameterizations of the cross sections of the 18 leading nuclear reactions in the BBN network using current experimental data compiled by EXFOR. We made an assumption about the α dependence of the penetration factors which differs from the Gamow-factor form that was used in previous investigations and used novel estimates for the Coulomb contribution to nuclear binding energies based on a recent *ab initio* calculation in the framework of NLEFT in order to determine the α-dependence of the nuclear binding energies and the corresponding Q-values. A further new ingredient for studying the α-dependence of the weak β-decays in the BBN network is a novel value for the electromagnetic contribution to the neutron–proton mass difference, which is slightly smaller than what has been used before. All these new inputs were then used to determine the variation of the reaction rates with varying α. Here, we found in particular that the variation of the reaction rates depends on the temperature, a feature that seems to have been ignored in previous investigations. We found consistent results with all four codes mentioned above and hence conclude that the model-dependence concerning the specific treatment of the BBN network is of minor importance for the α-dependence of the primordial abundances studied here. The results for the linear response do, however, deviate significantly from older results, in particular for the α-dependence of the abundances of $^3\mathrm{H} + ^3\mathrm{He}$ and $^7\mathrm{Li} + ^7\mathrm{Be}$, the former being much larger and the latter much smaller than found previously. Unfortunately, in the standard Big Bang scenario used here, the nominal abundance ratio $Y_{^7\mathrm{Li}+^7\mathrm{Be}}/Y_\mathrm{H}$ exceeds the current observationally based determination by a factor of three, a feature known as the lithium-problem that is not solved in the present treatment. This then also impedes a determination of consistent bounds on the value of the fine-structure constant from all available primordial abundance data. Using the observations for $^2\mathrm{H}$ and $^4\mathrm{He}$ alone, we can nevertheless state that these data would limit a possible variation of α to $|\delta_\alpha| < 0.02$. This is a stronger bound than found earlier in comparable investigations.

An investigation of the kind presented here heavily relies on the modeling of electromagnetic effects in the cross section data (or, equivalently the astrophysical S-factors) of the relevant nuclear reactions in the BBN-network. Here we opted for a specific form of Coulomb penetration factors that differ from Gamow-factors used before and stressed the relevance of the temperature dependence of the variation of α in the reaction rates that resulted from numerically integrating $\gamma(\alpha; T) \propto \int_0^\infty \mathrm{d}E\, E\, \sigma(\alpha; E)\, \exp(E/kT)$. It seems that further progress with the purpose of using primordial nucleosynthesis as a laboratory for exploring our understanding of fundamental physics, apart from astrophysical or cosmological aspects will be feasible only if *ab initio* theories describing the relevant nuclear reactions including electromagnetic effects become available. NLEFT appears to be a promising framework for doing just that, see *e.g.* Refs. [50,51].

Note added in proof: Very recently, a new `python` code that simulates BBN was published under the name `PRyMordial` [192,193]. Implementing changes due to a variation of α according to the method outlined above in `PRyMordial`, we could, accounting for some differences due to *e.g.* the absence of β-decay rates in `PRyMordial`, confirm the results obtained with the other four codes.

Acknowledgements We are grateful to Serdar Elhatisari for providing the expectation values of the electromagnetic contribution to the binding energies of the nuclei considered here. Furthermore we thank Jürg Gasser, Heiri Leutwyler and Andreas Nogga for pointing out relevant references. This project is part of the ERC Advanced Grant "EXOTIC" supported the European Research Council (ERC) under the European Union's Horizon 2020 research and innovation programme (grant agreement No. 101018170), We further acknowledge support by the Deutsche Forschungsgemeinschaft (DFG, German Research Foundation) and the NSFC through the funds provided to the Sino-German Collaborative Research Center TRR110 "Symmetries and the Emergence of Structure in QCD" (DFG Project ID 196253076 - TRR 110, NSFC Grant No. 12070131001), the Chinese Academy of Sciences (CAS) President's

International Fellowship Initiative (PIFI) (Grant No. 2018DM0034) and Volkswagen Stiftung (Grant No. 93562).

Funding Open Access funding enabled and organized by Projekt DEAL.

Data Availability Statement This manuscript has no associated data or the data will not be deposited. [Authors' comment: All relevant data are given in the tables. Additional date are available upon request].

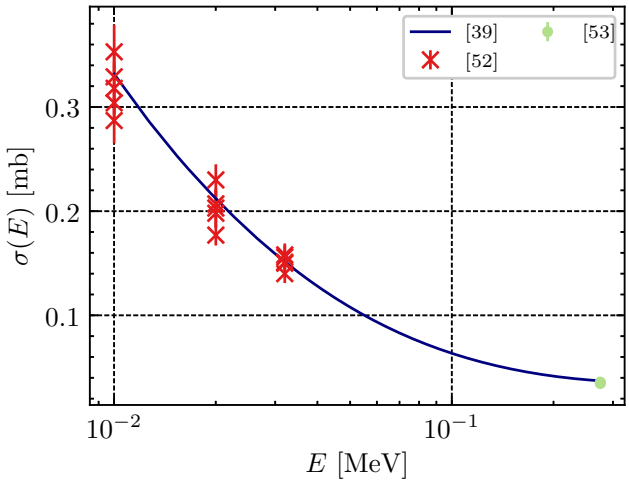

Fig. 9 Calculation of the cross section for the $n + p \rightarrow d + \gamma$ reaction by [39] compared to experimental data compiled by [54]

Appendix A: Parameterizations for *S*-factors and cross sections

For the relevant reactions treated here almost all S-factors, related to the cross section σ as

$$S(E) = E\,\sigma(E)\,\mathrm{e}^{\sqrt{E_G^i/E}} \tag{A1}$$

with E_G^i given by Eq. (32), can be written as

$$S(E) = S_0\,R(E; a_1, a_2, a_3, q_1, q_2, q_3)\,, \tag{A2}$$

with S_0 in units of MeV mb, and where

$$R(E; a_1, a_2, a_3, q_1, q_2, q_3) := \frac{1 + a_1\,E + a_2\,E^2 + a_3\,E^3}{1 + q_1\,E + q_2\,E^2 + q_3\,E^3}\,, \tag{A3}$$

is a rational function of the center-of-mass (CMS) kinetic energy E (given in MeV). There are, however, some reactions where resonances occur in the energy range considered here. For these, we can parameterize the S-factor as the rational function of Eq. (A3) combined with relativistic Breit–Wigner functions. The parameters for the relativistic Breit–Wigner functions of the form

$$BW(E; b, \Gamma, M) = \frac{b}{\Gamma^2 M^2 + \left(E^2 - M^2\right)^2} \tag{A4}$$

can be found in Table 11, where E, Γ and M are given in MeV. The use of a non-relativistic Breit–Wigner function of the form

$$bw(E; b, \kappa, M) = \frac{b}{1 + \kappa\,(E - M)^2} \tag{A5}$$

was found to be more appropriate for the reactions $^7\mathrm{Li} + d \rightarrow n + {}^4\mathrm{He} + {}^4\mathrm{He}$ and $^7\mathrm{Be} + n \rightarrow {}^7\mathrm{Li} + p$, the corresponding parameters (κ in MeV^{-2}) can also be found in Table 11.

A.1 The $n + p \rightarrow d + \gamma$ reaction

The cross section for the leading nuclear reaction of BBN, namely $n + p \rightarrow d + \gamma$, was calculated according to the formulas, *viz.* Eqs. (3.3)–(3.16) given in [39] with the parame-

Table 8 Fit parameters of the S-factor, see Eq.(A1), according to Eqs. (A2, A3) and Eq. (A6) for radiative capture reactions. S_0 is given in MeV mb; a_k and q_k in units of MeV^{-k}

Reaction	S_0		a_1	a_2	a_3	q_1	q_2	q_3
$d + p \rightarrow {}^3\mathrm{He} + \gamma$	2.066	$\times 10^{-4}$	30.431	14.943	0	− 0.032	0.035	0
$d + {}^4\mathrm{He} \rightarrow {}^6\mathrm{Li} + \gamma$	3.162	$\times 10^{-6}$	−3.163	15.271	− 0.633	0	0	0
$^3\mathrm{H} + p \rightarrow {}^4\mathrm{He} + \gamma$	1.875	$\times 10^{-3}$	10.773	32.613	113.836	0	0	8.919×10^{-3}
$^3\mathrm{H} + {}^4\mathrm{He} \rightarrow {}^7\mathrm{Li} + \gamma$	1.057	$\times 10^{-1}$	−1.378	1.106	0	0.128	0	0
$^3\mathrm{He} + {}^4\mathrm{He} \rightarrow {}^7\mathrm{Be} + \gamma$	4.912	$\times 10^{-1}$	−0.908	0.336	0	− 0.610	0.247	0
$^6\mathrm{Li} + p \rightarrow {}^7\mathrm{Be} + \gamma$	5.000	$\times 10^{-2}$	−13.863	53.532	14.977	− 10.907	33.652	0

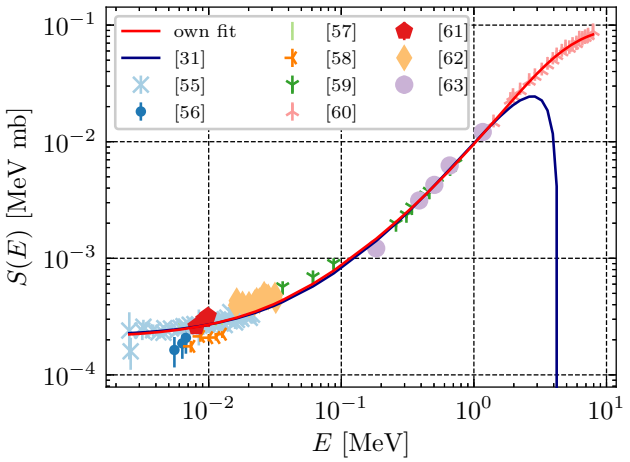

Fig. 10 Fit (red curve, color online) of the S-factor for the $d + p \rightarrow {}^3\mathrm{He} + \gamma$ reaction compared to data compiled by EXFOR [54]

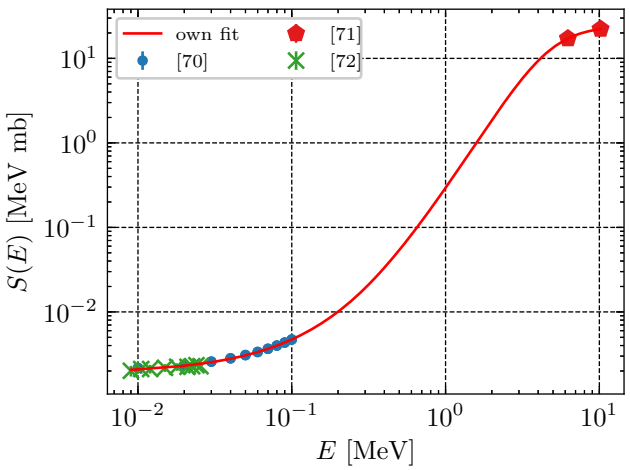

Fig. 11 Fit (red curve, color online) of the S-factor for the ${}^3\mathrm{H} + p \rightarrow {}^4\mathrm{He} + \gamma$ reaction compared to data compiled by EXFOR [54]

ters quoted there, also see Sect. 2.6. In Fig. 9 this description is compared to the existing data as compiled in [54].

A.2 Other radiative capture reactions

The parameters found by a fit of the parameters in Eqs. (A2, A3) to the data are displayed in Table 8 for most radiative capture reactions treated here.

The parameterizations are compared to experimental data compiled by EXFOR [54] in Figs. 10, 11, 12, 13 and 14.

The only exception is the reaction $d + {}^4\mathrm{He} \rightarrow {}^6\mathrm{Li} + \gamma$, where a resonance appears. In this case the S-factor is given by the sum of a cubic polynomial in E and a relativistic Breit–Wigner function:

$$S(E) = S_0 \left(1 + a_1 E + a_2 E^2 + a_3 E^3\right) + BW(E; b, \Gamma, M) \quad \text{(A6)}$$

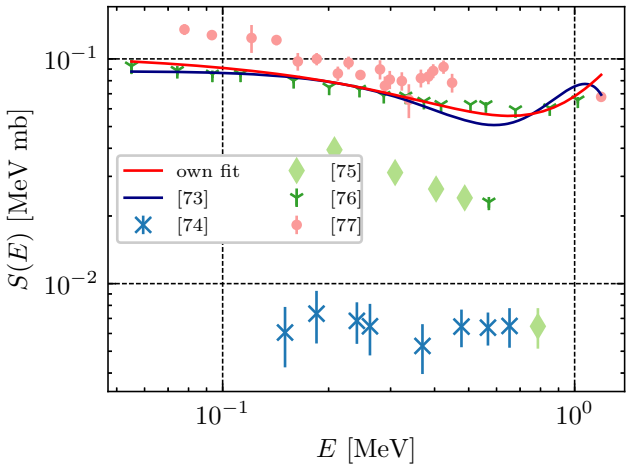

Fig. 12 Fit (red curve, color online) of the S-factor for the ${}^3\mathrm{H}+{}^4\mathrm{He} \rightarrow {}^7\mathrm{Li} + \gamma$ reaction compared to data compiled by EXFOR [54]

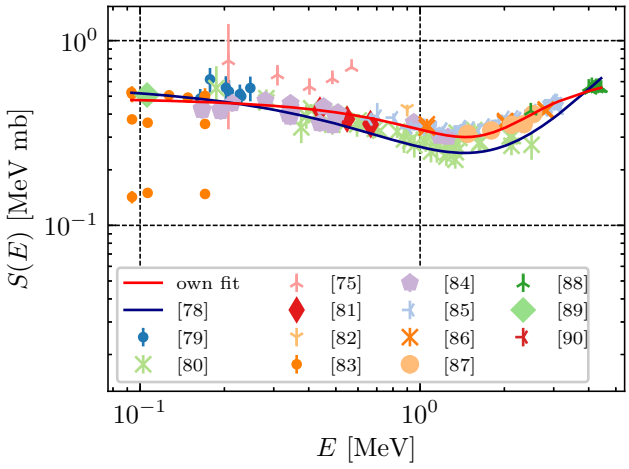

Fig. 13 Fit (red curve, color online) of the S-factor for the ${}^3\mathrm{He} + {}^4\mathrm{He} \rightarrow {}^7\mathrm{Be} + \gamma$ reaction compared to data compiled by EXFOR [54]

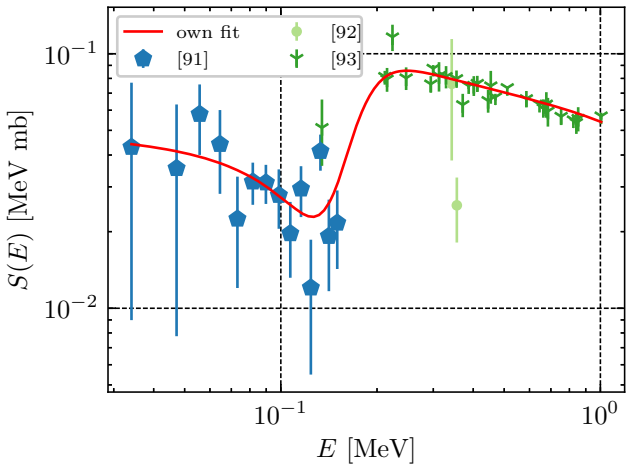

Fig. 14 Fit (red curve, color online) of the S-factor for the ${}^6\mathrm{Li} + p \rightarrow {}^7\mathrm{Be} + \gamma$ reaction compared to data compiled by EXFOR [54]

Table 9 Fit parameters of the S-factor, see Eq.(A1), according to Eqs. (A2, A3, A7, A8) and (A9) for charged particle reactions. S_0 is given in MeV mb; a_k and q_k in units of MeV^{-k}. For these reactions $q_3 = 0$

Reaction	Energy range	S_0	a_1	a_2	a_3	q_1	q_2
$d + d \rightarrow {}^3\mathrm{He} + n$		54.908	6.942	0.378	0	0.636	− 0.018
$d + d \rightarrow p + {}^3\mathrm{H}$		70.667	27.281	136.744	0	38.369	9.531
${}^3\mathrm{H} + d \rightarrow n + {}^4\mathrm{He}$	$E < 0.28$ MeV	10800.846	− 1.974	18.252	0	− 24.464	244.175
	$E \geq 0.28$ MeV	− 2116.168	0.137	0.527	− 0.038	− 8.747	0
${}^3\mathrm{He} + d \rightarrow p + {}^4\mathrm{He}$	$E < 0.25$ MeV	6703.216	− 8.823	27.654	− 2.772	− 9.380	24.921
	$E \geq 0.25$ MeV	10663.275	− 0.899	1.562	− 0.033	− 6.664	20.204
${}^6\mathrm{Li} + p \rightarrow {}^3\mathrm{He} + {}^4\mathrm{He}$		288.587	− 0.305	− 1.494	0.981	0	0
${}^7\mathrm{Li} + p \rightarrow {}^4\mathrm{He} + {}^4\mathrm{He}$	$E \leq 4.1$ MeV	338.062	0.731	− 0.102	0	0	0
	$E > 4.1$ MeV	12312.399	− 0.472	0.057	0	0	0
${}^7\mathrm{Be} + d \rightarrow p + {}^4\mathrm{He} + {}^4\mathrm{He}$		684.412	− 0.554	0.142	0	− 0.535	0.077
${}^7\mathrm{Li} + d \rightarrow n + {}^4\mathrm{He} + {}^4\mathrm{He}$		2968.470	8.279	− 0.308	0	54.611	0

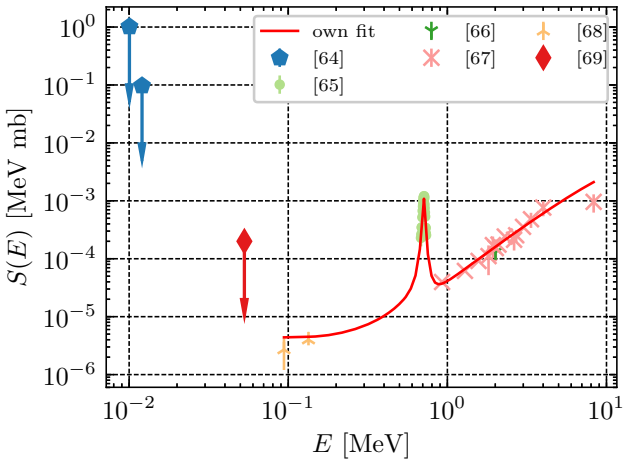

Fig. 15 Fit (red curve, color online) of the S-factor for the $d + {}^4\mathrm{He} \rightarrow {}^6\mathrm{Li} + \gamma$ reaction compared to data compiled by EXFOR [54]. The three upper limits for $E < 0.1$ MeV, denoted by arrows, were not included in the fit

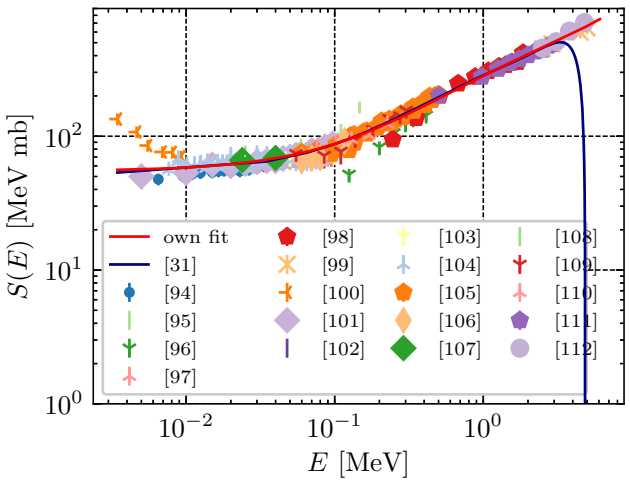

Fig. 16 Fit (red curve, color online) of the S-factor for the $d + d \rightarrow {}^3\mathrm{He} + n$ reaction compared to data compiled by EXFOR [54]

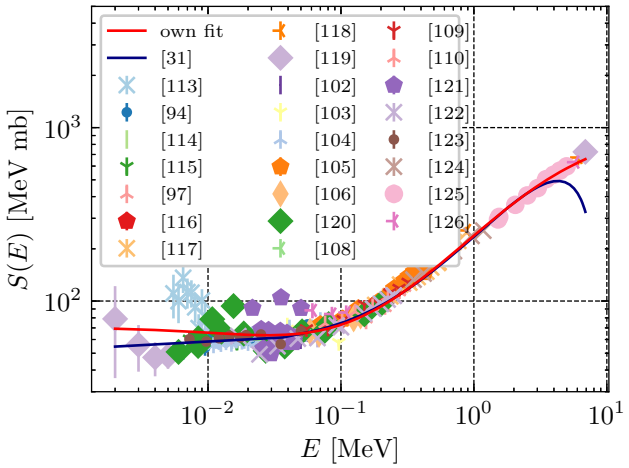

Fig. 17 Fit (red curve, color online) of the S-factor for the $d + d \rightarrow p + {}^3\mathrm{H}$ reaction compared to data compiled by EXFOR [54]

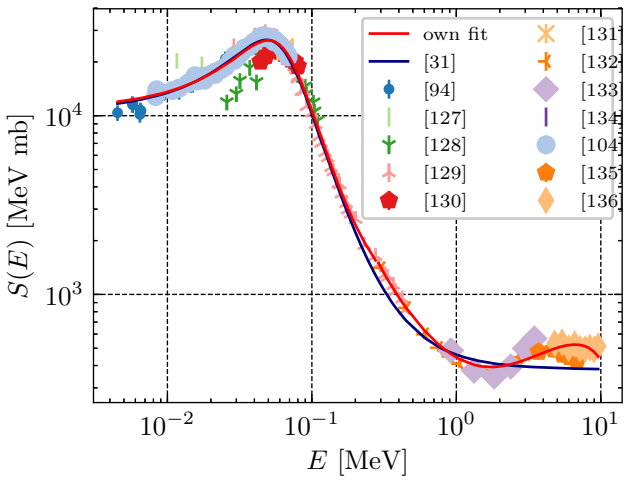

Fig. 18 Fit (red curve, color online) of the S-factor for the ${}^3\mathrm{H} + d \rightarrow n + {}^4\mathrm{He}$ reaction compared to data compiled by EXFOR [54]

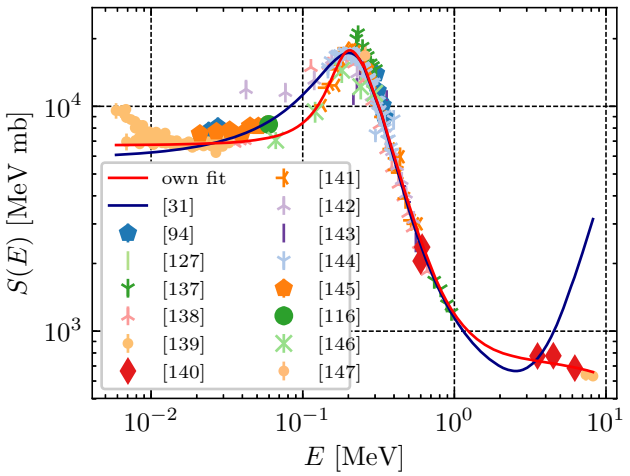

Fig. 19 Fit (red curve, color online) of the S-factor for the $^3\mathrm{He}+d \rightarrow p+{}^4\mathrm{He}$ reaction compared to data compiled by EXFOR [54]

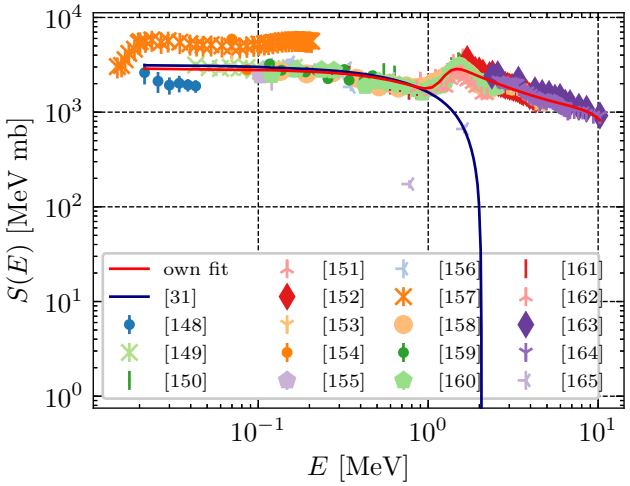

Fig. 20 Fit (red curve, color online) of the S-factor for the $^6\mathrm{Li}+p \rightarrow {}^3\mathrm{He}+{}^4\mathrm{He}$ reaction compared to data compiled by EXFOR [54]

with the parameters listed in Tables 8 and 11. This parameterization is compared to experimental data compiled by EXFOR [54] in Fig. 15.

A.3 Charged particle reactions

As in Section A2, we fitted the S-factors according to Eqs. (A2, A3). The parameters are displayed in Table 9 for most charged particle reactions treated here.

For the reaction $^6\mathrm{Li}+p \rightarrow {}^3\mathrm{He}+{}^4\mathrm{He}$ which has two resonances, the S-factor is given by an expression of the form

$$S(E) = S_0 \left(1 + a_1 E + a_2 E^2 + a_3 E^3\right) \times BW(E; b_1, \Gamma_1, M_1) \times BW(E; b_2, \Gamma_2, M_2) \tag{A7}$$

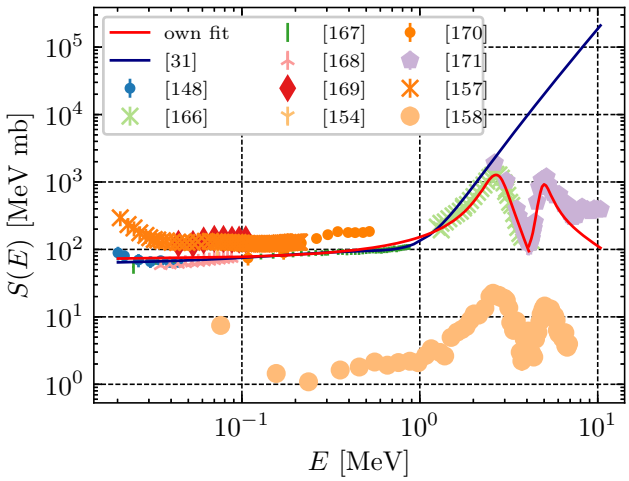

Fig. 21 Fit (red curve, color online) of the S-factor for the $^7\mathrm{Li}+p \rightarrow {}^4\mathrm{He}+{}^4\mathrm{He}$ reaction compared to data compiled by EXFOR [54]

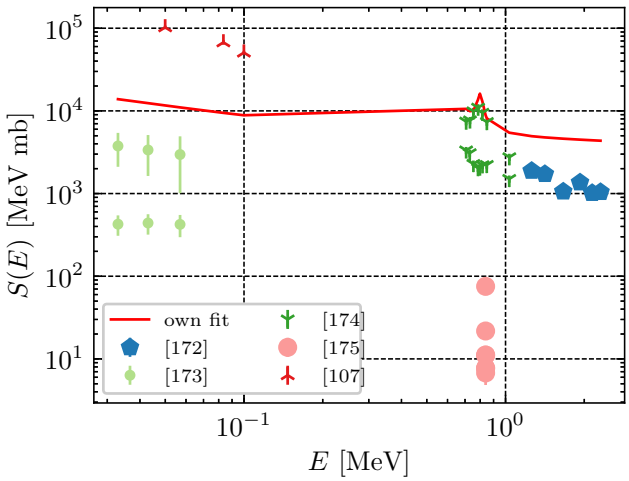

Fig. 22 Fit (red curve, color online) of the S-factor for the $^7\mathrm{Li}+d \rightarrow n+{}^4\mathrm{He}+{}^4\mathrm{He}$ reaction compared to data compiled by EXFOR [54]

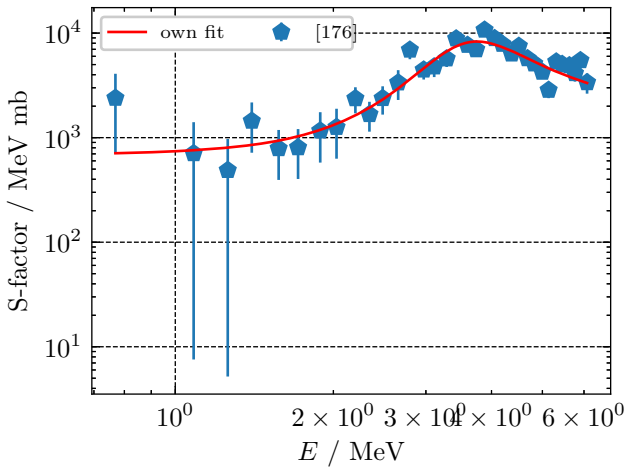

Fig. 23 Fit (red curve, color online) of the S-factor for the $^7\mathrm{Be}+d \rightarrow p+{}^4\mathrm{He}+{}^4\mathrm{He}$ reaction compared to data compiled by EXFOR [54]

Table 10 Fit parameters of the function $S^{[n]}$, see Eq. (A10), according to Eqs. (A12, A3) neutron-induced reactions. $S_0^{[n]}$ is given in MeV$^{1/2}$ mb, and a_k and q_k in units of MeV^{-k}

Reaction	Energy range	$S_0^{[n]}$	a_1	a_2	a_3	q_1	q_2	q_3
$^3\mathrm{He}+n \rightarrow p+{}^3\mathrm{H}$	$E \leq 2.8$ MeV	715	20.814	0	6.8	38.681	27.876	12.637
	$E > 2.8$ MeV	1691.556[a]	− 0.280	0.033	− 0.001	− 0.234	0.024	0
$^7\mathrm{Be}+n \rightarrow {}^4\mathrm{He}+{}^4\mathrm{He}$	$E \leq 2.0$ MeV	0.381	22.875	7.931	0	0	0	0
	$E > 2.0$ MeV	− 0.418	− 108.504	79.576	− 15.092	0	0	0

[a]Here $S_0^{[n]}$ in units of MeV mb; to be divided by $\sqrt{E}$, E in MeV. in order to yield $S^{[n]}$

and for the reaction $^7\mathrm{Li}+p \rightarrow {}^4\mathrm{He}+{}^4\mathrm{He}$ with one resonance the S-factor is given by

$$S(E) = S_0 \left(1 + a_1 E + a_2 E^2 + a_3 E^3\right) \times BW(E; b_1, \Gamma_1, M_1)\,. \tag{A8}$$

For the reaction $^7\mathrm{Li}+d \rightarrow n+{}^4\mathrm{He}+{}^4\mathrm{He}$ a parameterization of the form

$$S(E) = S_0 \frac{1 + a_1\,E + a_2\,E^2}{1 + q_1\,E} + bw(E; b_1, \kappa_1, M_1) + bw(E; b_2, \kappa_2, M_2) \tag{A9}$$

was used. The parameters of the Breit–Wigner functions can be found in Table 11.

These S-factor fits are compared to experimental data compiled by in EXFOR [54] in Figs. 16, 17, 18, 19, 20, 21, 22 and 23.

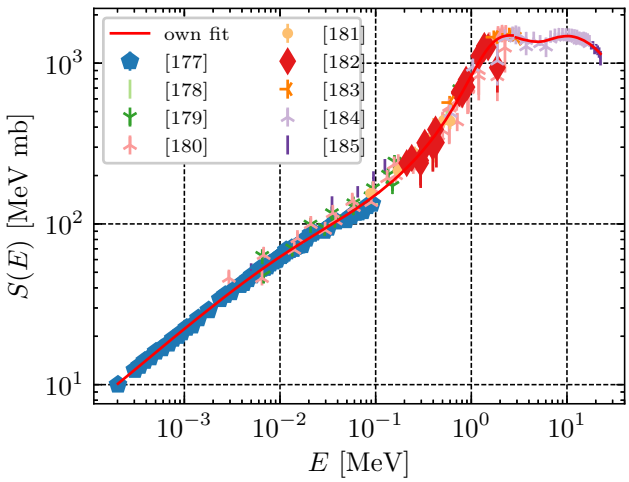

Fig. 24 Fit (red curve, color online) of $S(E) = S^{[n]}(E)\sqrt{E}$ for the $^3\mathrm{He}+n \rightarrow p+{}^3\mathrm{H}$ reaction compared to data compiled by EXFOR [54]

A.4 Neutron-induced reactions

For neutron capture reactions the cross section is written as

$$\sigma(E) = S^{[n]}(E)/\sqrt{E}, \tag{A10}$$

implying that the function $S^{[n]}$ is given in units of (MeV)$^{1/2}$ mb. The S-factor then reads

$$S(E) = \sigma(E)\,E = S^{[n]}(E)\,\sqrt{E}\,, \tag{A11}$$

since for neutron-induced reactions the Gamow-factor is unity. For neutron-induced reactions we give parameterizations of $S^{[n]}(E)$ in terms of

$$S_0^{[n]}\,R(E; a_1, a_2, a_3, q_1, q_2, q_3) \tag{A12}$$

Table 11 Fit parameters for resonances parameterized as Breit–Wigner functions in Eqs. (A4, A5). Γ_k and M_k in MeV; κ_k in MeV^{-2}. The units for b_k and c depend on the context, see Eqs. (A6, A7, A8, A9)

Reaction	Energy range	b_1	Γ_1	M_1	b_2	Γ_2	M_2	c
$d+{}^4\mathrm{He} \rightarrow {}^6\mathrm{Li}+\gamma$		4.310×10^{-7}	0.028	0.711				
$^6\mathrm{Li}+p \rightarrow {}^3\mathrm{He}+{}^4\mathrm{He}$		5113.917	0.654	1.187	104.696	13.972	8.72	0
$^7\mathrm{Li}+p \rightarrow {}^4\mathrm{He}+{}^4\mathrm{He}$	$E \leq 4.1$ MeV	12.395	1.012	2.669				
	$E > 4.1$ MeV	27.448	0.912	4.824				
$^7\mathrm{Be}+n \rightarrow {}^4\mathrm{He}+{}^4\mathrm{He}$	$E \leq 2.0$ MeV	4.023	0.825	0.887	2.035	0.455	3.482	0.156
	$E > 2.0$ MeV	9.331	1.246	1.346	39.447	0.723	3.114	− 0.023
		b_1	κ_1	M_1	b_2	κ_2	M_2	c
$^7\mathrm{Li}+d \rightarrow n+{}^4\mathrm{He}+{}^4\mathrm{He}$		9820.6	82.387	0.6	8991.0	1963.84	0.8	0
$^7\mathrm{Be}+n \rightarrow {}^7\mathrm{Li}+p$		1.116	131.7	0.327	0	0	0	0

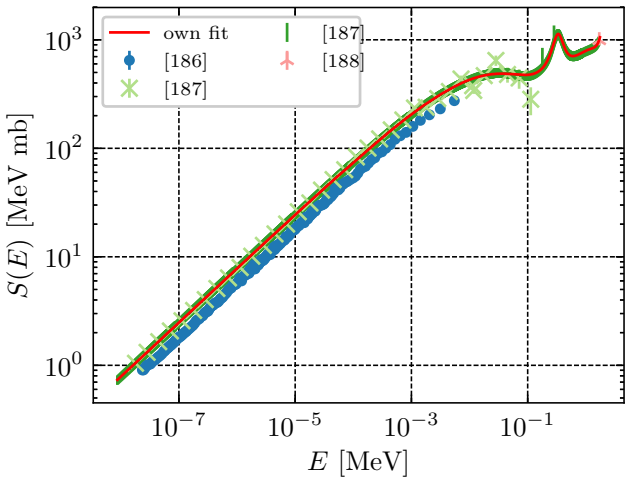

Fig. 25 Fit (red curve, color online) of $S(E) = S^{[n]}(E)\sqrt{E}$ for the $^7\mathrm{Be} + n \rightarrow p + {}^7\mathrm{Li}$ reaction compared to data compiled by EXFOR [54]

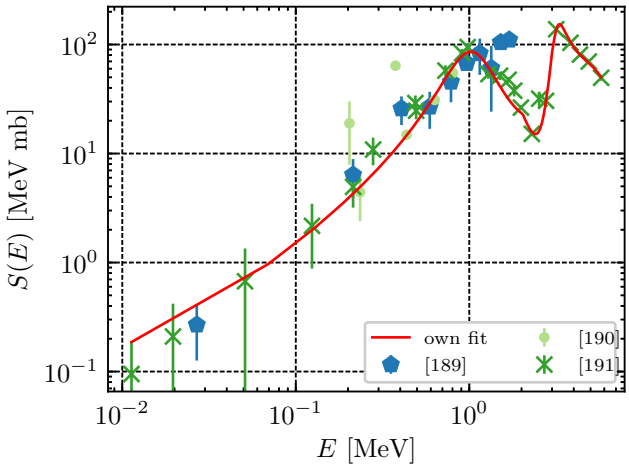

Fig. 26 Fit (red curve, color online) of $S(E) = S^{[n]}(E)\sqrt{E}$ for the $^7\mathrm{Be} + n \rightarrow {}^4\mathrm{He} + {}^4\mathrm{He}$ reaction compared to data compiled by EXFOR [54]

with the rational function R of Eq. (A3) and the Breit–Wigner functions of Eqs. (A4, A5). $S_0^{[n]}$ is then given in units of $\mathrm{MeV}^{1/2}$ mb.

Note that for the reaction $^3\mathrm{He} + n \rightarrow p + {}^3\mathrm{H}$ for $E > 2.8$ MeV, the rational polynomial described by the coefficients in Table 10 still needs to be divided by $\sqrt{E}$. For this reaction the fit of the S-factor is compared to experimental data compiled by EXFOR [54] in Fig. 24.

For the reaction $^7\mathrm{Be} + n \rightarrow p + {}^7\mathrm{Li}$ the following parameterization in terms of a non-relativistic Breit–Wigner function and a polynomial in $\sqrt{E}$ was used:

$$S^{[n]}(E) = 1000.0 \times \begin{cases} bw(E; b, \kappa, M) + 7.7874 - 47.778\, E^{\frac{1}{2}} \\ \quad +140.00\, E - 222.87\, E^{\frac{3}{2}} \\ \quad +201.84\, E^2 - 97.983\, E^{\frac{5}{2}} \\ \quad +19.773\, E^3 \ (\mathrm{MeV})^{1/2} \quad \mathrm{mb}\,, \\ E \leq 2.0\,\mathrm{MeV}\,, \\ 1139.627\ (\mathrm{MeV})^{1/2} \quad \mathrm{mb}\,, \\ E > 2.0\,\mathrm{MeV} \end{cases} \tag{A13}$$

where again the CMS energy E is given in MeV and the parameters of the Breit–Wigner function can be found in Table 11. For this reaction the S-factor fit is compared to experimental data compiled by EXFOR [54] in Fig. 25.

Finally, the form of the parameterization for the reaction $^7\mathrm{Be} + n \rightarrow {}^4\mathrm{He} + {}^4\mathrm{He}$ reads

$$S^{[n]}(E) = S_0^{[n]} \left(1 + a_1\, E + a_2\, E^2 + a_3\, E^3\right) \times \big(c + BW(E; b_1, \Gamma_1, M_1) + BW(E; b_2, \Gamma_2, M_2)\big)\,. \tag{14}$$

The S-factor is compared to experimental data compiled by EXFOR [54] in Fig. 26.

References

1. P.A.M. Dirac, Proc. Roy. Soc. Lond. A **333**, 403–418 (1973). https://doi.org/10.1098/rspa.1973.0070
2. K.A. Bronnikov, V.D. Ivashchuk, V.V. Khrushchev, Meas. Tech. **65**(3), 151–156 (2022). https://doi.org/10.1007/s11018-022-02062-z. arXiv:2210.13187 [hep-ph]
3. R.P. Gupta, Symmetry **15**(2), 259 (2023). https://doi.org/10.3390/sym15020259. arXiv:2301.09795 [astro-ph.CO]
4. F. Iocco, G. Mangano, G. Miele, O. Pisanti, P.D. Serpico, Phys. Rept. **472**, 1–76 (2009). https://doi.org/10.1016/j.physrep.2009.02.002. arXiv:0809.0631 [astro-ph]
5. J. P. Uzan, Living Rev. Rel. **14**, 2 (2011). https://doi.org/10.12942/lrr-2011-2 arXiv:1009.5514 [astro-ph.CO]
6. F.C. Adams, Phys. Rept. **807**, 1–111 (2019). https://doi.org/10.1016/j.physrep.2019.02.001. arXiv:1902.03928 [astro-ph.CO]
7. L. Bergstrom, S. Iguri, H. Rubinstein, Phys. Rev. D **60**, 045005 (1999). https://doi.org/10.1103/PhysRevD.60.045005. arXiv:astro-ph/9902157 [astro-ph]
8. K.M. Nollett, R.E. Lopez, Phys. Rev. D **66**, 063507 (2002). https://doi.org/10.1103/PhysRevD.66.063507. arXiv:astro-ph/0204325 [astro-ph]
9. A. Coc, N.J. Nunes, K.A. Olive, J.P. Uzan, E. Vangioni, Phys. Rev. D **76**, 023511 (2007). https://doi.org/10.1103/PhysRevD.76.023511. arXiv:astro-ph/0610733 [astro-ph]
10. T. Dent, S. Stern, C. Wetterich, Phys. Rev. D **76**, 063513 (2007). https://doi.org/10.1103/PhysRevD.76.063513. arXiv:0705.0696 [astro-ph]
11. U.-G. Meißner, Sci. Bull. **60**(1), 43–54 (2015). https://doi.org/10.1007/s11434-014-0670-2. arXiv:1409.2959 [hep-th]
12. J.F. Donoghue, Ann. Rev. Nucl. Part. Sci. **66**, 1–21 (2016). https://doi.org/10.1146/annurev-nucl-102115-044644. arXiv:1601.05136 [hep-ph]
13. L. E. Marcucci, G. Mangano, A. Kievsky, M. Viviani, Phys. Rev. Lett. **116** (2016) no.10, 102501 [erratum: Phys. Rev. Lett. **117** (2016) no.4, 049901] https://doi.org/10.1103/PhysRevLett.116.102501 arXiv:1510.07877 [nucl-th]

14. J. Dohet-Eraly, P. Navrátil, S. Quaglioni, W. Horiuchi, G. Hupin, F. Raimondi, Phys. Lett. B **757**, 430–436 (2016). https://doi.org/10.1016/j.physletb.2016.04.021. [arXiv:1510.07717 [nucl-th]]
15. R. Higa, G. Rupak, A. Vaghani, Eur. Phys. J. A **54** (2018) no.5, 89 https://doi.org/10.1140/epja/i2018-12486-5 [arXiv:1612.08959 [nucl-th]]
16. P. Premarathna, G. Rupak, Eur. Phys. J. A **56** (2020) no.6, 166 https://doi.org/10.1140/epja/s10050-020-00113-z [arXiv:1906.04143 [nucl-th]]
17. R. Higa, P. Premarathna, G. Rupak, Phys. Rev. C **106** (2022) no.1, 014601 https://doi.org/10.1103/PhysRevC.106.014601
18. C. Hebborn, G. Hupin, K. Kravvaris, S. Quaglioni, P. Navrátil, P. Gysbers, Phys. Rev. Lett. **129**(4), 042503 (2020). https://doi.org/10.1103/PhysRevLett.129.042503. [arXiv:2203.15914 [nucl-th]]
19. U.-G. Meißner, B.Ch. Metsch, Eur. Phys. J. A **58**, 212 (2022). https://doi.org/10.1140/epja/s10050-022-00869-6. [arXiv:2208.12600 [nucl-th]]
20. L. Kawano, *Let's go: Early universe. 2. Primordial nucleosynthesis:The Computer way.* Report FERMILAB-PUB-92-004-A (1992)
21. A. Arbey, Comput. Phys. Commun. **183**, 1822–1831 (2012). https://doi.org/10.1016/j.cpc.2012.03.018. [arXiv:1106.1363 [astro-ph.CO]]
22. A. Arbey, J. Auffinger, K.P. Hickerson, E.S. Jenssen, Comput. Phys. Commun. **248**, 106982 (2020). https://doi.org/10.1016/j.cpc.2019.106982. [arXiv:1806.11095 [astro-ph.CO]]
23. O. Pisanti, A. Cirillo, S. Esposito, F. Iocco, G. Mangano, G. Miele, P.D. Serpico, Comput. Phys. Commun. **178**, 956–971 (2008). https://doi.org/10.1016/j.cpc.2008.02.015. [arXiv:0705.0290 [astro-ph]]
24. R. Consiglio, P.F. de Salas, G. Mangano, G. Miele, S. Pastor, O. Pisanti, Comput. Phys. Commun. **233**, 237–242 (2018). https://doi.org/10.1016/j.cpc.2018.06.022. [arXiv:1712.04378 [astro-ph.CO]]
25. S. Gariazzo, P.F. de Salas, O. Pisanti, R. Consiglio, Comput. Phys. Commun. **271**, 108205 (2022). https://doi.org/10.1016/j.cpc.2021.108205. [arXiv:2103.05027 [astro-ph.IM]]
26. C. Pitrou, A. Coc, J.P. Uzan, E. Vangioni, Phys. Rept. **754**, 1–66 (2018). https://doi.org/10.1016/j.physrep.2018.04.005. [arXiv:1801.08023 [astro-ph.CO]]
27. J. Humblet, Nucl. Phys. **50**, 1–16 (1964). https://doi.org/10.1016/0029-5582(64)90188-9
28. J.P. Jeukenne, Nucl. Phys. **58**, 1 (1964). https://doi.org/10.1016/0029-5582(64)90516-4
29. J. Humblet, W.A. Fowler, R.A. Zimmerman, Astron. Astrophys. **177**, 317–325 (1987)
30. R. L. Workman *et al.* [Particle Data Group], PTEP **2022**, 083C01 (2022). https://doi.org/10.1093/ptep/ptac097
31. P.D. Serpico, S. Esposito, F. Iocco, G. Mangano, G. Miele, O. Pisanti, J. Cosmol. Astropart. Phys. **2004**(12), 10 (2004). https://doi.org/10.1088/1475-7516/2004/12/010. [arXiv:astro-ph/0408076 [astro-ph]]
32. E. Segrè, *Nuclei and Particles*, (2nd Edition, Benjamin, Reading, 1977)
33. M. Morita, *Beta Decay and Muon Capture* (Benjamin, Reading MA, 1973)
34. J. Gasser, H. Leutwyler, A. Rusetsky, Eur. Phys. J. C **80**(12), 1121 (2020). https://doi.org/10.1140/epjc/s10052-020-08615-2. [arXiv:2008.05806 [hep-ph]]
35. J. Gasser, H. Leutwyler, A. Rusetsky, Phys. Lett. B **814**, 136087 (2021). https://doi.org/10.1016/j.physletb.2021.136087. [arXiv:2003.13612 [hep-ph]]
36. J. Gasser, H. Leutwyler, Nucl. Phys. B **94**, 269–310 (1975). https://doi.org/10.1016/0550-3213(75)90493-9
37. U.-G. Meißner, A. Rusetsky, *Effective Field Theories* (Cambridge University Press, 2022)
38. J.W. Chen, M.J. Savage, Phys. Rev. C **60**, 065205 (1999). https://doi.org/10.1103/PhysRevC.60.065205. [arXiv:nucl-th/9907042 [nucl-th]]
39. G. Rupak, Nucl. Phys. A **678**, 405–423 (2000). https://doi.org/10.1016/S0375-9474(00)00323-7. [arXiv:nucl-th/9911018 [nucl-th]]
40. R.B. Wiringa, V.G.J. Stoks, R. Schiavilla, Phys. Rev. C **51**, 38–51 (1995). https://doi.org/10.1103/PhysRevC.51.38. [arXiv:nucl-th/9408016 [nucl-th]]
41. C.J. Hogan, Rev. Mod. Phys. **72**, 1149–1161 (2000). https://doi.org/10.1103/RevModPhys.72.1149. [arXiv:astro-ph/9909295 [astro-ph]]
42. J. Gasser, H. Leutwyler, Phys. Rept. **87**, 77–169 (1982). https://doi.org/10.1016/0370-1573(82)90035-7
43. D. Benzaid, S. Bentridi, A. Kerraci, N. Amrani, Nucl. Sci. Tech. **31**(1), 9 (2020). https://doi.org/10.1007/s41365-019-0718-8
44. S. Elhatisari *et al.*, [arXiv:2210.17488 [nucl-th]]
45. W.J. Huang, M. Wang, F.G. Kondev, G. Audi, S. Naimi, Chin. Phys. C **45**(3), 030002 (2021). https://doi.org/10.1088/1674-1137/abddb0
46. Y. Xu, S. Goriely, A. Jorissen, G. Chen, M. Arnould, Astron. Astrophys. **549**, A106 (2013). https://doi.org/10.1051/0004-6361/201220537. [arXiv:1212.0628 [nucl-th]]
47. S. Goriely, S. Hilaire, A.J. Koning, Astron. Astrophys. **487**, 767 (2008). https://doi.org/10.1051/0004-6361:20078825. [arXiv:0806.2239 [astro-ph]]
48. E. Epelbaum, H. Krebs, T.A. Lähde, D. Lee, U.-G. Meißner, Eur. Phys. J. A **49**, 82 (2013). https://doi.org/10.1140/epja/i2013-13082-y. [arXiv:1303.4856 [nucl-th]]
49. T.A. Lähde, U.-G. Meißner, E. Epelbaum, Eur. Phys. J. A **56**(3), 89 (2020). https://doi.org/10.1140/epja/s10050-020-00093-0. [arXiv:1906.00607 [nucl-th]]
50. S. Elhatisari, D. Lee, G. Rupak, E. Epelbaum, H. Krebs, T.A. Lähde, T. Luu, U.-G. Meißner, Nature **528**, 111 (2015). https://doi.org/10.1038/nature16067. [arXiv:1506.03513 [nucl-th]]
51. S. Elhatisari, T.A. Lähde, D. Lee, U.-G. Meißner, T. Vonk, JHEP **02**, 001 (2022). https://doi.org/10.1007/JHEP02(2022)001. [arXiv:2112.09409 [hep-th]]
52. T.S. Suzuki, Y. Nagai, T. Shima et al., Astrophys. J. **439**, L59 (1995). https://doi.org/10.1086/187744
53. Y. Nagai, T.S. Suzuki, T. Kikuchi et al., Phys. Rev. C **56**, 3173–3179 (1997). https://doi.org/10.1103/PhysRevC.56.3173
54. V. Zerkin, B. Pritychenko, Nucl. Instrum. Methods A **888**, 31–43 (2018). https://doi.org/10.1016/j.nima.2018.01.045
55. C. Casella, H. Costantini, A. Lemut et al., Nucl. Phys. A **706**(1), 203–216 (2002). https://doi.org/10.1016/S0375-9474(02)00749-2
56. V. M. Bystritsky, V. V. Gerasimov, A. R. Krylov *et al.*, Bull. Acad. Sci. USSR, Phys. **74**, 531–534 (2010). https://doi.org/10.3103/S1062873810040234
57. V.M. Bystritsky et al., Nucl. Instrum. Meth. A **753**, 91–96 (2014). https://doi.org/10.1016/j.nima.2014.03.059
58. V.M. Bystritsky et al., Nucl. Instrum. Meth. A **737**, 248–252 (2014). https://doi.org/10.1016/j.nima.2013.11.072
59. G.M. Bailey, G.M. Griffiths, M.A. Olivo et al., Can. J. Phys. **48**(24), 3059–3061 (1970). https://doi.org/10.1139/p70-379
60. W. Wölfli, R. Bösch, J. Lang, Helv. Phys. Acta **40**, 946 (1967). https://doi.org/10.5169/seals-113803
61. V. Bystritsky, V. Gerasimov, A. Krylov et al., Nucl. Instrum. Methods A **595**(3), 543–548 (2008). https://doi.org/10.1016/j.nima.2008.07.152
62. G.M. Griffiths, M. Lal, C.D. Scarfe, Can. J. Phys. **41**(5), 724–736 (1963). https://doi.org/10.1139/p63-077
63. G.M. Griffiths, E.A. Larson, L.P. Robertson, Can. J. Phys. **40**(4), 402–411 (1962). https://doi.org/10.1139/p62-045

64. Y.B. Burkatovskaya et al., Phys. Part. Nucl. Lett. **13**(2), 190–197 (2016). https://doi.org/10.1134/S1547477116020059
65. P. Mohr, V. Kölle, S. Wilmes et al., Phys. Rev. C **50**, 1543–1549 (1994). https://doi.org/10.1103/PhysRevC.50.1543
66. J.C. Kim, J. Korean Phys. Soc. **15**, 101 (1982)
67. R.G.H. Robertson, P. Dyer, R.A. Warner et al., Phys. Rev. Lett. **47**, 1867–1870 (1981). https://doi.org/10.1103/PhysRevLett.47.1867
68. M. Anders, D. Trezzi, R. Menegazzo et al., Phys. Rev. Lett. **113**, 042501 (2014). https://doi.org/10.1103/PhysRevLett.113.042501
69. F.E. Cecil, J. Yan, C.S. Galovich, Phys. Rev. C **53**, 1967–1970 (1996). https://doi.org/10.1103/PhysRevC.53.1967
70. R.S. Canon, S.O. Nelson, K. Sabourov et al., Phys. Rev. C **65**, 044008 (2002). https://doi.org/10.1103/PhysRevC.65.044008
71. J.R. Calarco, S.S. Hanna, C.C. Chang et al., Phys. Rev. C **28**, 483–488 (1983). https://doi.org/10.1103/PhysRevC.28.483
72. V.A. Varlachev, G.N. Dudkin, B.A. Nechaev et al., JETP Lett. **113**(4), 231–237 (2021). https://doi.org/10.1134/S0021364021040111
73. R.H. Cyburt, Phys. Rev. D **70**, 023505 (2004). https://doi.org/10.1103/PhysRevD.70.023505
74. G.M. Griffiths, J.B. Warren, R.A. Morrow et al., Can. J. Phys. **39**(10), 1397–1408 (1961). https://doi.org/10.1139/p61-167
75. H.D. Holmgren, R.L. Johnston, Phys. Rev. **113**, 1556–1559 (1959). https://doi.org/10.1103/PhysRev.113.1556
76. C.R. Brune, R.W. Kavanagh, C. Rolfs, Phys. Rev. C **50**, 2205–2218 (1994). https://doi.org/10.1103/PhysRevC.50.2205
77. U. Schröder, A. Redder, C. Rolfs et al., Phys. Lett. B **192**, 55–58 (1987). https://doi.org/10.1016/0370-2693(87)91141-5
78. R. H. Cyburt, B. Davids, Phys. Rev. C **78**, 064,614 (2008). https://doi.org/10.1103/PhysRevC.78.064614
79. K. Nagatani, M.R. Dwarakanath, D. Ashery, Nucl. Phys. A **128**, 325–332 (1969). https://doi.org/10.1016/0375-9474(69)90995-6
80. P.D. Parker, R.W. Kavanagh, Phys. Rev. **131**, 2578–2582 (1963). https://doi.org/10.1103/PhysRev.131.2578
81. M. Hilgemeier, H.W. Becker, C. Rolfs et al., Z. Phys. A **329**, 243–254 (1988). https://doi.org/10.1007/BF01283781
82. R.G.H. Robertson, P. Dyer, T.J. Bowles et al., Phys. Rev. C **27**, 11–17 (1983). https://doi.org/10.1103/PhysRevC.27.11
83. H. Costantini et al., Nucl. Phys. A **814**, 144–158 (2008). https://doi.org/10.1016/j.nuclphysa.2008.09.014
84. J.L. Osborne, C.A. Barnes, R.W. Kavanagh et al., Nucl. Phys. A **419**, 115–132 (1984). https://doi.org/10.1016/0375-9474(84)90288-4
85. A. Di Leva, L. Gialanella, R. Kunz *et al.*, Phys. Rev. Lett. **102**, 232,502 (2009). https://doi.org/10.1103/PhysRevLett.102.232502
86. M. Carmona-Gallardo, B. S. Nara Singh, M. J. G. Borge *et al.*, Phys. Rev. C **86**, 032,801 (2012). https://doi.org/10.1103/PhysRevC.86.032801
87. C. Bordeanu, G. Gyürky, Z. Halász et al., Nucl. Phys. A **908**, 1–11 (2013). https://doi.org/10.1016/j.nuclphysa.2013.03.012
88. T. Szücs, G. G. Kiss, G. Gyürky *et al.*, Phys. Rev. C **99**, 055,804 (2019). https://doi.org/10.1103/PhysRevC.99.055804
89. G. Gyürky, F. Confortola, H. Costantini et al., Phys. Rev. C **75**, 035805 (2007). https://doi.org/10.1103/PhysRevC.75.035805
90. T.K. Alexander, G.C. Ball, W.N. Lennard et al., Nucl. Phys. A **427**, 526–544 (1984). https://doi.org/10.1016/0375-9474(84)90229-X
91. R. Bruss, O. Arkis, H. Bucka *et al.*, Proceedings of the Second International Symposium on Nuclear Astrophysics, Karlsruhe, 1992, edited by F. Käppeler and K. Wisshak (Institute of Physics Publishing, 1992) p. 169
92. S. Bashkin, R.R. Carlson, Phys. Rev. **97**, 1245–1249 (1955). https://doi.org/10.1103/PhysRev.97.1245
93. Z.E. Switkowski, J.C.P. Heggie, D.L. Kennedy et al., Nucl. Phys. A **331**, 50–60 (1979). https://doi.org/10.1016/0375-9474(79)90300-2
94. W.R. Arnold, J.A. Phillips, G.A. Sawyer et al., Phys. Rev. **93**, 483–497 (1954). https://doi.org/10.1103/PhysRev.93.483
95. J.H. Manley, H.M. Agnew, H.H. Barschall et al., Phys. Rev. **70**, 602–605 (1946). https://doi.org/10.1103/PhysRev.70.602
96. P.R. Chagnon, G.E. Owen, Phys. Rev. **101**, 1798–1803 (1956). https://doi.org/10.1103/PhysRev.101.1798
97. N. Ying, B.B. Cox, B.K. Barnes et al., Nucl. Phys. A **206**, 481–497 (1973). https://doi.org/10.1016/0375-9474(73)90080-8
98. G.T. Hunter, H.T. Richards, Phys. Rev. **76**, 1445–1449 (1949). https://doi.org/10.1103/PhysRev.76.1445
99. S.T. Thornton, Nucl. Phys. A **136**, 25–34 (1969). https://doi.org/10.1016/0375-9474(69)90036-0
100. A.S. Belov, V.E. Kusik, Y.V. Ryabov, Nuovo Cimento A **103**, 1647–1650 (1990). https://doi.org/10.1007/BF02820309
101. V. A. Davidenko, A. M. Kucher, I. S. Pogrebov *et al.*, At. Energ. [Sov. J. At. Energy] 7 (1957)
102. R.E. Brown, N. Jarmie, Phys. Rev. C **41**, 1391–1400 (1990). https://doi.org/10.1103/PhysRevC.41.1391
103. U. Greife, F. Gorris, M. Junker et al., Z. Phys. A **351**, 107–112 (1995). https://doi.org/10.1007/BF01292792
104. T. F. R. Group and T. F. R. Division, High. Energ. Phys. Nuc. **9**, 723 (1985)
105. A. S. Ganeev, A. M. Govorov, G. M. Osetinkii *et al.*, At. Energ. [Sov. J. At. Energy] 26 (1957)
106. K.G. McNeill, G.M. Keyser, Phys. Rev. **81**, 602–606 (1951). https://doi.org/10.1103/PhysRev.81.602
107. M.A. Hofstee, A.K. Pallone, F.E. Cecil et al., Nucl. Phys. A **688**, 527–529 (2001). https://doi.org/10.1016/S0375-9474(01)00777-1
108. D.L. Booth, G. Preston, P.F.D. Shaw, Proc. Phys. Soc. A **69**, 265 (1956). https://doi.org/10.1088/0370-1298/69/3/309
109. D. S. Leonard, H. J. Karwowski, C. R. Brune *et al.*, Phys. Rev. C **73**, 045,801 (2006). https://doi.org/10.1103/PhysRevC.73.045801
110. G. Preston, P. F. D. Shaw, S. A. Young *et al.*, Proc. R. Soc. London, Ser. A **226**(1165), 206–216 (1954). https://doi.org/10.1098/rspa.1954.0249
111. R.L. Schulte, M. Cosack, A.W. Obst et al., Nucl. Phys. A **192**, 609–624 (1972). https://doi.org/10.1016/0375-9474(72)90093-0
112. M.D. Goldberg, J.M. Le Blanc, Phys. Rev. **119**, 1992–1999 (1960). https://doi.org/10.1103/PhysRev.119.1992
113. W. Tie-Shan, Y. Zhen, H. Yunemura et al., Chin. Phys. Lett. **24**(11), 3103 (2007). https://doi.org/10.1088/0256-307X/24/11/024
114. J.H. Sanders, J. Moffat, D. Roaf, Phys. Rev. **77**, 754 (1950)
115. J. Moffatt, D. Roaf, J. H. Sanders *et al.*, Proc. R. Soc. London, Ser. A **212**(1109), 220–234 (1952). https://doi.org/10.1098/rspa.1952.0077
116. A. Krauss, H.W. Becker, H.P. Trautvetter et al., Nucl. Phys. A **465**, 150–172 (1987). https://doi.org/10.1016/0375-9474(87)90302-2
117. V. V. Volkov, P. E. Vorotnikov, E. A. Koltypin *et al.*, At. Energ. [Sov. J. At. Energy] 15 (1957)
118. J.E. Brolley, T.M. Putnam, L. Rosen, Phys. Rev. **107**, 820–824 (1957). https://doi.org/10.1103/PhysRev.107.820
119. A. von Engel, C. C. . Goodyear, B. Bleaney, Proc. R. Soc. London, Ser. A **264**(1319), 445–457 (1961). https://doi.org/10.1098/rspa.1961.0210
120. P. A. Davenport, T. O. Jeffries, M. E. Owen *et al.*, Proc. R. Soc. London, Ser. A **216**(1124), 66–71 (1953). https://doi.org/10.1098/rspa.1953.0007
121. C.F. Cook, J.R. Smith, Phys. Rev. **89**, 785–786 (1953). https://doi.org/10.1103/PhysRev.89.785

122. W.A. Wenzel, W. Whaling, Phys. Rev. **88**, 1149–1154 (1952). https://doi.org/10.1103/PhysRev.88.1149
123. E. Bretscher, A.P. French, F.G.P. Seidl, Phys. Rev. **73**, 815–821 (1948). https://doi.org/10.1103/PhysRev.73.815
124. W. Grüebler, V. König, P.A. Schmelzbach et al., Nucl. Phys. A **369**, 381–395 (1981). https://doi.org/10.1016/0375-9474(81)90026-9
125. W. Grüebler, V. König, P.A. Schmelzbach et al., Nucl. Phys. A **193**, 129–148 (1972). https://doi.org/10.1016/0375-9474(72)90240-0
126. G. A. C., E. R. Graves, J. H. Coon *et al.*, Phys. Rev. **70**, 101 (1946)
127. R. G. Jarvis, D. Roaf, L. Cherwell, Proc. R. Soc. London, Ser. A **218**(1134), 432–438 (1953). https://doi.org/10.1098/rspa.1953.0116
128. V. A. Davidenko, I. S. Poerebou, A. I. Saukov, At. Energ. [Sov. J. At. Energy] **2**, 386 (1957)
129. E. M. Balabanov, I. J. Barit, L. N. Kacaurov *et al.*, At. Energ. [Sov. J. At. Energy] 57 (1957)
130. D. L. Allan, M. J. Poole, J. D. Cockcroft, Proceedings of the Royal Society of London. Series A. Mathematical and Physical Sciences Proc. R. Soc. London, Ser. A **204**(1079), 488–499 (1951). https://doi.org/10.1098/rspa.1951.0005
131. J.P. Conner, T.W. Bonner, J.R. Smith, Phys. Rev. **88**, 468–473 (1952). https://doi.org/10.1103/PhysRev.88.468
132. S.J. Bame, J.E. Perry, Phys. Rev. **107**, 1616–1620 (1957). https://doi.org/10.1103/PhysRev.107.1616
133. A. Galonsky, C.H. Johnson, Phys. Rev. **104**, 421–425 (1956). https://doi.org/10.1103/PhysRev.104.421
134. R.E. Brown, N. Jarmie, G.M. Hale, Phys. Rev. C **35**, 1999–2004 (1987). https://doi.org/10.1103/PhysRevC.35.1999
135. M.D. Goldberg, J.M. Le Blanc, Phys. Rev. **122**, 164–168 (1961). https://doi.org/10.1103/PhysRev.122.164
136. E. Magiera, M. Bormann, W. Scobel et al., Nucl. Phys. A **246**, 413–424 (1975). https://doi.org/10.1016/0375-9474(75)90656-9
137. G. Freier, H. Holmgren, Phys. Rev. **93**, 825–826 (1954). https://doi.org/10.1103/PhysRev.93.825
138. T.W. Bonner, J.P. Conner, A.B. Lillie, Phys. Rev. **88**, 473–476 (1952). https://doi.org/10.1103/PhysRev.88.473
139. S. Engstler, A. Krauss, K. Neldner et al., Phys. Lett. B **202**, 179–184 (1988). https://doi.org/10.1016/0370-2693(88)90003-2
140. L. Stewart, J.E. Brolley, L. Rosen, Phys. Rev. **119**, 1649–1653 (1960). https://doi.org/10.1103/PhysRev.119.1649
141. L. Zhichang, Y. Jingang, D. Xunliang, Yuanzineng Kexue Jishu/At. Energy. Sci. Technol. **11**, 229 (1977)
142. M.L. Cognata, C. Spitaleri, A. Tumino et al., Phys. Rev. C **72**, 065802 (2005). https://doi.org/10.1103/PhysRevC.72.065802
143. H. Erramli, T. Sauvage, M. Rhazi et al., Phys. Chem. News **23**, 67 (2005)
144. W. H. Geist, C. R. Brune, H. J. Karwowski *et al.*, Phys. Rev. C **60**, 054,003 (1999). https://doi.org/10.1103/PhysRevC.60.054003
145. J.L. Tuck, W.R. Arnold, J.A. Phillips et al., Phys. Rev. **88**, 159 (1952)
146. D. L. Booth, R. S. Hill, F. V. Price *et al.*, Proceedings of the Physical Society. Section A Proc. Phys. Soc. London, Sec. A **70**(12), 863 (1957). https://doi.org/10.1088/0370-1298/70/12/303
147. J.L. Yarnell, R.H. Lovberg, W.R. Stratton, Phys. Rev. **90**, 292–297 (1953). https://doi.org/10.1103/PhysRev.90.292
148. O. Fiedler, P. Kunze, Nucl. Phys. A **96**, 513–520 (1967). https://doi.org/10.1016/0375-9474(67)90601-X
149. W. Gemeinhardt, D. Kamke, C. von Rhöneck, Z. Phys. **197**, 58–74 (1966). https://doi.org/10.1007/BF01333086
150. J.B. Marion, G. Weber, F.S. Mozer, Phys. Rev. **104**, 1402–1407 (1956). https://doi.org/10.1103/PhysRev.104.1402
151. B. W. Hooton, M. Ivanovich, A.E.R.E Harwell Reports **18**, 37 (1972)
152. J.M.F. Jeronymo, G.S. Mani, A. Sadeghi, Nucl. Phys. **43**, 424 (1963). https://doi.org/10.1016/0029-5582(63)90364-X
153. U. Fasoli, D. Toniolo, G. Zago, Phys. Lett. **8**, 127 (1964). https://doi.org/10.1016/0031-9163(64)90737-1
154. J. Cruz et al., Phys. Lett. B **624**, 181–185 (2005). https://doi.org/10.1016/j.physletb.2005.08.036
155. M. Várnagy, J. Csikai, J. Szabó et al., Nucl. Instrum. Methods **119**, 451 (1974). https://doi.org/10.1016/0029-554X(74)90796-4
156. T. Shinozuka, Y. Tanaka, K. Sugiyama, Nucl. Phys. A **326**, 47–54 (1979). https://doi.org/10.1016/0375-9474(79)90365-8
157. G. A. Sawyer, J. A. Phillips, Los Alamos Scientific Lab. Reports **1578** (1953)
158. A. Tumino, C. Spitaleri, A. Di Pietro *et al.*, Phys. Rev. C **67**, 065,803 (2003). https://doi.org/10.1103/PhysRevC.67.065803
159. J.U. Kwon, J.C. Kim, B.N. Sung, Nucl. Phys. A **493**, 112–123 (1989). https://doi.org/10.1016/0375-9474(89)90535-6
160. A.J. Elwyn, R.E. Holland, C.N. Davids et al., Phys. Rev. C **20**, 1984–1992 (1979). https://doi.org/10.1103/PhysRevC.20.1984
161. F. Bertrand, G. Grenier, J. Pornet, Centre d'Etudes Nucleaires, Saclay **3428** (1968)
162. L. Chia-Shou, H. Wan-Shou, W. Min et al., Nucl. Phys. A **275**, 93–99 (1977). https://doi.org/10.1016/0375-9474(77)90277-9
163. G. M. Temmer, Proceedings of the Conference on Direct Interactions & Nuclear Reaction Mechanisms, Padua, 1962 (edited by E. Clementel and C. Villi, 1963) p. 1013
164. C. R. Gould, R. O. Nelson, J. R. Williams *et al.*, Nucl. Sci. Eng. **55**(3), 267–272 (1974). https://doi.org/10.13182/NSE74-A23453
165. H. Spinka, T. Tombrello, H. Winkler, Nucl. Phys. A **164**, 1–10 (1971). https://doi.org/10.1016/0375-9474(72)90803-2
166. Y. Cassagnou, J.M.F. Jeronymo, G.S. Mani et al., Nucl. Phys. **33**, 449 (1962). https://doi.org/10.1016/0029-5582(62)90537-0
167. C. Rolfs, R.W. Kavanagh, Nucl. Phys. A **455**, 179–188 (1986). https://doi.org/10.1016/0375-9474(86)90351-9
168. M. Spraker, R. M. Prior, M. A. Godwin *et al.*, Phys. Rev. C **61**, 015,802 (1999). https://doi.org/10.1103/PhysRevC.61.015802
169. C.C. Lee, J. Korean Phys. Soc. **2**, 1 (1969)
170. D.M. Ciric, R.V. Popic, R.B. Zakula et al., Rev. Res. **6**, 115 (1976)
171. G.S. Mani, R. Freeman, F. Picard et al., Nucl. Phys. **60**, 588 (1964). https://doi.org/10.1016/0029-5582(64)90095-1
172. G. M. Osetinskii, B. Sikora, Y. Tyke *et al.*, Joint. Inst. for Nucl. Res., Dubna **5143** (1970)
173. A. Sabourov, M.W. Ahmed, M.A. Blackston et al., Phys. Rev. C **73**, 015801 (2006). https://doi.org/10.1103/PhysRevC.73.015801
174. C. Nussbaum, Helv. Phys. Acta **42**, 361 (1969)
175. J. Catalá, R. Font, P. Senent et al., Nuovo Cimento **9**, 377–380 (1958). https://doi.org/10.1007/BF02747678
176. N. Rijal, I. Wiedenhöver, J.C. Blackmon et al., Phys. Rev. Lett. **122**, 182701 (2019). https://doi.org/10.1103/PhysRevLett.122.182701
177. S. B. Borzakov, K. Maletski, L. B. Pikelner *et al.*, Yad. Fiz. [Sov. J. Nucl. Phys.] **35**, 532 (1982)
178. D. G. Costello, S. J. Friesenhahn, W. M. Lopez, Nucl. Sci. Eng. **39**(3), 409–410 (1970). https://doi.org/10.13182/NSE70-A20005
179. R. L. Macklin, J. H. Gibbons, Proceedings of the International Conference on the Study of Nuclear Structure with Neutrons, Antwerp, 1965 (North-Holland, 1966) p. 13
180. J.H. Gibbons, R.L. Macklin, Phys. Rev. **114**, 571–580 (1959). https://doi.org/10.1103/PhysRev.114.571
181. R. Batchelor, R. Aves, T.H.R. Skyrme, Rev. Sci. Instrum. **26**(11), 1037–1047 (1955). https://doi.org/10.1063/1.1715182
182. J.H. Coon, Phys. Rev. **80**, 488–488 (1950). https://doi.org/10.1103/PhysRev.80.488
183. A.R. Sayres, K.W. Jones, C.S. Wu, Phys. Rev. **122**, 1853–1863 (1961). https://doi.org/10.1103/PhysRev.122.1853
184. B. Haesner, W. Heeringa, H.O. Klages et al., Phys. Rev. C **28**, 995–999 (1983). https://doi.org/10.1103/PhysRevC.28.995

185. R.G. Pizzone et al., Eur. Phys. J. A **56**(8), 199 (2020). https://doi.org/10.1140/epja/s10050-020-00212-x
186. P.E. Koehler, C.D. Bowman, F.J. Steinkruger et al., Phys. Rev. C **37**, 917–926 (1988). https://doi.org/10.1103/PhysRevC.37.917
187. L. Damone, M. Barbagallo, M. Mastromarco et al., Phys. Rev. Lett. **121**, 042701 (2018). https://doi.org/10.1103/PhysRevLett.121.042701
188. J. Červená, V. Havránek, V. Hnatowicz et al., Czech. J. Phys. **39**, 1263–1266 (1989). https://doi.org/10.1007/BF01605326
189. L. Lamia, M. Mazzocco, R.G. Pizzone et al., Astrophys. J. **879**(1), 23 (2019). https://doi.org/10.3847/1538-4357/ab2234
190. T. Kawabata, Y. Fujikawa, T. Furuno et al., Phys. Rev. Lett. **118**, 052701 (2017). https://doi.org/10.1103/PhysRevLett.118.052701
191. S.Q. Hou, J.J. He, S. Kubono et al., Phys. Rev. C **91**, 055802 (2015). https://doi.org/10.1103/PhysRevC.91.055802
192. A.-K. Burns, T. M. P. Tait, M. Valli, arXiv:2307.07061 [hep-ph] (2023)
193. A.-K. Burns, T. M. P. Tait, M. Valli, https://github.com/vallima/PRyMordial